THESIS FOR THE DEGREE OF DOCTOR OF PHILOSOPHY IN NATURAL SCIENCE,
WITH FOCUS ON CHEMISTRY

Selectivity in the Chlorate Process:
Hydrogen Evolution and Hypochlorite Reduction on Chromium Oxide/Hydroxide

Adriano Soares de Oliveira Gomes
Department of Chemistry and Molecular Biology
Faculty of Science

ISBN: 978-91-629-0434-0 (TRYCKT)
ISBN: 978-91-629-0435-7 (PDF)
Available on-line at: http://handle.net/2077/55067

DEPARTMENT OF CHEMISTRY AND
MOLECULAR BIOLOGY

Selectivity in the Chlorate Process: Hydrogen Evolution and Hypochlorite Reduction on Chromium Oxide/Hydroxide

Adriano Soares de Oliveira Gomes

Cover illustration: The selective mechanism provided by $Cr(OH)_3$ towards the hydrogen evolution reaction.

Department of Chemistry and Molecular Biology
University of Gothenburg
412 96 Gothenburg, Sweden

ISBN: 978-91-629-0434-0 (TRYCKT)
ISBN: 978-91-629-0435-7 (PDF)
Available on-line at: http://handle.net/2077/55067

Printed by BrandFactory AB
Kållered, Sweden

"*Try to understand the last word of what the great artists, the serious masters, say in their masterpieces; God will be found there*"

Vincent van Gogh

Abstract

Production of chlorate is dependent of using sodium dichromate as a component in the electrolyte. Dichromate provides selectivity by forming a Cr(III) oxide-like film on the cathodes. Without dichromate, unwanted cathodic reactions dominate instead of the hydrogen evolution reaction (HER), and chlorate is not produced. However, Cr(VI) is a hazardous element and must be replaced in the process with a less harmful compound for environmental and safety reasons. Removing Cr(VI) from the chlorate process has proven to be challenging, and no replacement element or material has been found.

This thesis presents experimental and theoretical results leading to a mechanism that explains the selectivity between the unwanted reactions and the HER. The mechanism also supports previous findings regarding the Cr(III) film formed in situ on chlorate cathodes.

The approach in this work was to ex situ electrodeposit two structures, $Cr(OH)_3$ and Cr_2O_3, as pure films. These ex situ-formed films could then be characterized prior to investigating their electrochemical performance relevant to the chlorate process.

The morphology of the films were analysed by scanning electron microscopy, revealing clear differences. The $Cr(OH)_3$ film was thin and rough, while the Cr_2O_3 film was composed of plate-shaped crystallites with approximately 1 µm in length. The molecular structure was investigated by Raman spectroscopy. This was, to some extent, challenging by the discovery that $Cr(OH)_3$ converts to Cr_2O_3 at high laser energies. Still, the spectra collected with lower laser power clearly showed Raman signatures related to $Cr(OH)_3$.

Electrochemical investigations showed that hypochlorite reduction was blocked on both surfaces, $Cr(OH)_3$ and Cr_2O_3, indicating that the blocking effect is related to Cr(III) and not to the films' molecular structure or morphology. This reaction was also completely hindered by the $Cr(OH)_3$ deposited on more active electrodes towards hypochlorite reduction, as Fe or Au.

In contrast, the HER could still proceed on both Cr(III) films. Interestingly, on Cr_2O_3 the electrode activity was enhanced towards the HER, while $Cr(OH)_3$ displayed the opposite effect. These results show that the HER take place on the Cr-film, which must be taken in to account in the selective mechanism.

The blocking mechanism was first rationalized in the context of surface charge of Cr(III) oxide-like films and their p-type semiconducting properties. These properties may somewhat hinder the reduction of hypochlorite, but cannot give the full explanation for the selectivity. Further insights about the mechanism were given using DFT calculations and the complete selectivity mechanism was determined. Cr-sites cannot be reformed during hypochlorite reduction, and are irreversibly blocked by OH. Thus, the reduction of hypochlorite is blocked by OH groups strongly binding to the surface. The HER, however, can readily proceed at the OH covered surfaces.

Key words: sodium chlorate, hydrogen, sodium dichromate, hypochlorite, HER, mild steel electrodes, Cr_2O_3, $Cr(OH)_3$

Sammanfattning

Vid klorattillverkning är natriumdikromat en nödvändig komponent i elektrolyten. Utan dikromat förstörs produkten (klorat) samt dess reaktionsintermediär (hypoklorit) på katoden medan önskad vätgasutveckling uteblir. Kromat innehåller emellertid sexvärt krom som är giftigt, både för människa och miljö, och det finns en stark drivkraft att hitta andra alternativ. Att ersätta krom i kloratprocessen har visat sig vara mycket komplext och trots forskning under lång tid så finns det idag inga alternativ.

Denna avhandling beskriver experimentella och teoretiska resultat som leder till en mekanism som förklarar selektiviteten, dvs. hur hypokloritreduktion hindras och hur vätgasutveckling ändå kan ske. Den föreslagna mekanismen stödjer dessutom tidigare studier av kromats effekt på kloratkatoder.

I kloratprocessen reduceras dikromat på katoden och bildar en krom(III) film som ger upphov till önskad selektivitet för katoden. Ansatsen i denna avhandling har varit att elektrodeponera två förutbestämda krom(III)filmer (Cr_2O_3 och $Cr(OH)_3$) i ren form. Syftet var att möjliggöra en noggrann ytkarakterisering av dessa filmer innan elektrokemiska experiment, relevanta för kloratprocessen, genomfördes.

Morfologin hos de två filmerna karakteriserades med svepelektronmikroskopi där dessa uppvisade tydliga olikheter. $Cr(OH)_3$ var tunn med en rå yta, medan Cr_2O_3 visade plattliknande kristalliter, ca 1 µm långa. Ramanspektroskopi användes för att verifiera molekylstrukturen, vilket delvis försvårades av upptäckten att $Cr(OH)_3$ omvandlas till Cr_2O_3 vid höga laserenergier. Vid låga laserenergier kunde dock spektra med tydliga $Cr(OH)_3$ signaturer erhållas.

Elektrokemisk karakterisering av filmerna visade att reduktion av hypoklorit blockerades på såväl $Cr(OH)_3$ som Cr_2O_3. Detta indikerar att blockeringen är relaterad till Cr(III) som sådan, snarare än filmens molekylära sammansättning eller morfologi. Blockeringen var oberoende av vilket substrat som användes, Ti, Fe och Au. Hastigheten för vätgastveckling påverkades både av substrat och typ av kromfilm. Cr_2O_3 ökade aktiviteteten för vätgasutveckling medan $Cr(OH)_3$ gav motsatt effekt. Dessa resultat ger en stark indikation på att vattenreduktion sker på Cr-filmen vilket måste beaktas ur ett mekanistiskt perspektiv.

Mekanismen undersöktes i kontext av p-typ halvledaregenskaper samt ytladdning dessa faktorer kunde dock inte förklara selektiviteten. Mekanismen för selektiviteten studerades vidare med teoretiska DFT beräkningar. Genom dessa kunde en komplett beskrivning av selektiviteten hos Cr(III) filmer läggas fram. De aktiva sätena på Cr(III) filmen kan inte återbildas vid hypoklotritreduktion utan blir blockerade av OH grupper som binder irreversibelt till aktiva säten. Vätgasutveckling kan dock ske på denna yta.

Keywords: natriumklorat, vätgas, natriumdikromat, hypoklorit, HER, kolstål elektrod, Cr_2O_3, $Cr(OH)_3$

List of Publications

This thesis summarizes the work presented in the following papers.

Paper 1: **Study of Hypochlorite Reduction Related to the Sodium Chlorate Process**
K. Hedenstedt, A.S.O. Gomes, M. Busch and E. Ahlberg
Electrocatalysis, Vol.7, 4, pp. 326-335 (2016)
DOI 10.1007/s12678-016-0310-5

Paper 2: **Electrochemical Investigation of the Hydrogen Evolution Reaction on Electrodeposited Films of $Cr(OH)_3$ and Cr_2O_3 in Mild Alkaline Solutions**
A.S.O. Gomes, N. Simic, M. Wildlock, A. Martinelli and E. Ahlberg
Electrocatalysis
DOI 10.1007/s12678-017-0435-1

Paper 3: **Hydrogen Evolution at Mixed $Fe_{x-1}Cr_xOOH$**
P. Larses, A.S.O. Gomes, M. Busch and E. Ahlberg
Journal of Electroanalytical Chemistry and Interfacial Electrochemistry, in press
DOI 10.1016/j.jelechem.2017.09.032

Paper 4: **Understanding Selectivity in the Chlorate Process: a Step Towards Efficient Hydrogen Production**
A.S.O. Gomes, M. Busch, N. Simic, M. Wildlock and E. Ahlberg
Manuscript

Paper 5: **A Micro-Raman Spectroscopic Study of $Cr(OH)_3$ and Cr_2O_3 Nanoparticles Obtained by the Hydrothermal Method**
A.S.O. Gomes, N. Yaghini, A. Martinelli and E. Ahlberg
Journal of Raman Spectroscopy, Vol. 48, 10, pp. 1256-1263
DOI 10.1002/jrs.5198

Contribution List

Paper 1: I planned and performed electrochemical and surface characterization measurements and interpreted data from $Cr(OH)_3$ and Cr_2O_3 electrodeposition and hypochlorite reduction on bare Ti and on Ti covered with $Cr(OH)_3$ and Cr_2O_3. I contributed to writing of the paper.

Paper 2: I planned and performed all electrochemical and surface characterization measurements on $Cr(OH)_3$ and Cr_2O_3 supported on Ti electrodes. Results have been interpreted with help of the co-authors. I am the main author with support from co-authors.

Paper 3: I planned and performed electrochemical and surface characterization measurements of $Cr(OH)_3$ electrodeposition and hydrogen evolution reaction on Fe covered with $Cr(OH)_3$. I supported on electrochemical and surface characterization analyses and data interpretation from $Fe_{1-x}Cr_xOOH$ investigation. I contributed to writing of the paper.

Paper 4: I planned and performed all electrochemical and surface characterization measurements from $Cr(OH)_3$ electrodeposition on Au, Fe and Ti and the hydrogen evolution reaction on the pure metals and covered surfaces. I contributed in discussing DFT calculations. I am the main author with support from co-authors.

Paper 5: I planned and performed all synthesis and characterization of $Cr(OH)_3$ nanoparticles and Cr_2O_3 nanoparticles. I am the main author with support from co-authors.

Table of Contents

1. Introduction

Elemental chlorine-free (ECF) pulp bleaching is the state-of-the-art technology for sustainable pulp production [1]. Since more than 20 years, chlorine (Cl_2) has been phased out as a bleaching agent due to environmental reasons, and chlorine dioxide (ClO_2) has become the preferred bleaching chemical in ECF bleaching technology. The advantages of using ClO_2 compared to total chlorine-free (TCF) techniques include high selectivity during the cellulose delignification step, the yield of a pulp with high brightness and a low decrease in viscosity [2]. Most importantly, ECF eliminates the formation of toxic chlorinated organic compounds, such as those obtained with elemental chlorine [3]. Chlorine dioxide is thermodynamically unstable and must be produced at the site of use. The manufacture of chlorine dioxide proceeds via chemical reduction of sodium chlorate ($NaClO_3$). The preferred reducing agents are methanol or hydrogen peroxide, and the reaction is catalysed by acid (Equation 1). Chloride should be avoided as a reducing agent, as large amounts of elemental chlorine are formed. Approximately 95% of the total amount of sodium chlorate produced is used in large-scale chlorine dioxide production [1].

$$9NaClO_3 + 2CH_3OH + 6H_2SO_4 \rightarrow 9ClO_2 + 3Na_3H(SO_4)_2 + \frac{1}{2}CO_2 + \frac{3}{2}HCOOH + 7H_2O \quad (1)$$

Sodium chlorate is produced via the electrolysis of sodium chloride (Equation 2) [1, 4], which is one of the most important industrial electrochemical processes. Chlorate production requires large amounts of electricity, which leads to a high production cost. Most of this electrical energy is used in the cells that drive electrochemical reactions. The energy consumption can be lowered by finding the optimum process conditions, modifying the cell design or applying electrodes with high catalytic activity, i.e., electrodes that present a low overpotential towards target reactions. Furthermore, the electrodes should also be selective to avoid wasting energy through parasitic (unwanted) electrochemical reactions. In this sense, dimensionally stable anode (DSA) electrodes meet the demands of a perfect catalyst. DSAs provide outstanding activity and selectivity towards chlorine evolution, the main anodic reaction, and have revolutionized the chlorate [5] and chlor-alkali [5-7] industries since their invention in 1965 [8].

$$3H_2O + NaCl \xrightarrow{6e^-} NaClO_3 + 3H_2 \quad (2)$$

On the other side of the electrode gap, the most commonly used cathode for manufacturing chlorate is mild steel. Steel is a cost-efficient choice, with good mechanical stability and relatively low overpotential for water reduction. However, mild steel is not a selective electrode, and under normal electrolysis conditions, hypochlorite and chlorate reduction are thermodynamically favoured over water reduction [9, 10]. To supress side reactions, small amounts of hexavalent chromium (Cr(VI)) are added to the electrolyte as a sodium dichromate ($Na_2Cr_2O_7$) salt [4, 9, 11-16]. Alternative to Cr(VI), Cr(III) salts can also be added [17], which are converted in situ to Cr(VI) in the strongly oxidizing electrolyte. Hexavalent chromium provides high selectivity by forming a protective Cr(III) oxide-like film at the cathode surface. The film completely blocks side reactions, while allows water reduction to occur (see Section 2.4).

The mechanism by which Cr(III) oxide-like films hinder the reduction of hypochlorite has been the subject of several studies [9, 11, 12, 16, 18, 19]. Advances and flaws in these studies will be detailed later in this thesis. For now, it is enough to state that no study has been able to fully elucidate the blocking mechanism. Therefore, a deeper understanding of the mechanism is necessary, which is the subject of this thesis. The knowledge presented here can be the basis for the development of new selective materials so that Cr(VI) is no longer necessary during electrolysis. Such materials would represent a breakthrough in cathode technology for chlorate production similar to the breakthrough DSA presented for anodes 50 years ago.

The drive towards a new technology in which dichromate is not necessary is directed by the toxicity of Cr(VI) compounds [20]. Cr(VI) is acutely toxic, and it also has long-term effects to humans and to the environment. In total, Cr(VI) bears five out of the nine hazard symbols for chemicals (Figure 1). Thus, a replacement has long been pursued, but all attempts so far have failed [21-25]. Currently, a substitution for Cr(VI) has become more desired, as Cr(VI) has been added to the REACH list (Annex XIV) and thus essentially banned from use in the European Union (EU) [26]. Therefore, unless authorization is given for the continued use of hexavalent chromium, chlorate production within the EU will be gravely endangered. The discontinuing manufacturing of sodium chlorate in the EU would have significant negative economic impacts on the whole European pulp industry. Still, there is no available chlorate production technology in which dichromate is not needed.

Figure 1 – Chemical hazard symbols for Cr(VI) compounds (from left to right): oxidizing; toxic/acutely toxic; carcinogenic, mutagenic and/or reprotoxic; corrosive; and toxic to the environment.

This work investigates $Cr(OH)_3$ and Cr_2O_3 electrodeposited onto several substrates to identify properties essential for efficient chlorate production. Earlier works examined Cr(III) formed in situ, and thus, the film composition was not completely clear. The idea of depositing Cr(III) oxide-like films offers the opportunity to characterize the films prior to electrochemical analyses. Thus, interpretation of the results can be based on the structure and composition of the films. By fulfilling these objectives, a more fundamental understanding of the Cr(III) layers will be achieved. The experimental work was complemented along with density functional theory (DFT) calculations to obtain knowledge of the reaction mechanism on a molecular level. The combination of theory and experiments significantly improved the understanding of the mechanism for selectivity. This new knowledge increased the probability of finding other materials that provide the same critical characteristics as Cr(VI) to make the chlorate process safer and more environmentally friendly.

2. Sodium chlorate production

2.1. Process overview

The process for sodium chlorate production can be divided into five main steps (Figure 2) [1]. The first step is the dissolution of raw NaCl in the salt dissolver tank. Then, the brine enters the brine purification system, which consists of filters and ion exchangers, where solid particles and soluble impurities are removed. The purified brine is mixed with the electrolyte before entering the electrochemical cells (electrolysers). In the cells, electricity is applied to drive electrochemical reactions, which are followed by chemical reactions that form chlorate. The kinetics of bulk chlorate formation is relatively slow, and a reactor tank is needed between the electrolysers and the crystallization system (crystallizer) to allow completion of the reaction. The pH and temperature in the reactor tank are carefully controlled to obtain the highest reaction rate. Finally, the chlorate-rich electrolyte is fed into the crystallizer, where the electrolyte temperature is lowered and $NaClO_3$ is separated by precipitation.

As stated in the Introduction, sodium dichromate is an essential component in the electrolyte to achieve chlorate production. In present technologies, chlorate cannot be produced without the addition of dichromate. The process is hence operated as a closed-loop system to retain the dichromate in the process. Therefore, the electrolyte containing chloride, chlorate and dichromate return after the crystallizer to the main circulation loop. A drawback of the closed-loop operation is the presence of impurities in the main loop, which accumulate in the electrolyte over time. Impurities may cause cell potential increases, efficiency losses, risks of short circuits, and obstruction of the electrolyte flow in the cell gap (by build-up of solid deposits on the electrodes). Some impurities, such as nickel and copper, catalyse the decomposition of the reaction intermediates (hypochlorite and hypochlorous acid, Section 2.2), dramatically affecting the production yield. In the worst case scenario, an emergency shutdown is necessary to remove impurities from the electrolyte.

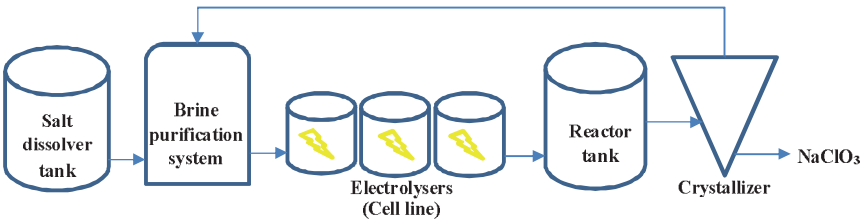

Figure 2 – Simplified sketch of a chlorate plant.

The cell line is the heart of the whole process and consists of several electrolysers units connected in series. The number of electrolysers and cell lines vary according to the technology and/or plant capacity. The chlorate cells are undivided, meaning that the cathode and anode share the same electrolyte, with no membrane in between. The electrode setup can be monopolar, bipolar or multi-monopolar (Figure 2) [27] inside rectangular or cylindrical cell box configurations. Monopolar technology has the advantage of simplicity, while bipolar technology affords a higher capacity per electrolyser [27]. Multi-monopolar technology combines the advantages of both monopolar and bipolar setups [27]. Cells are designed to be robust and to facilitate the electrolyte flow and current distribution to minimize cost and optimize production. In chlorate manufacturing, electricity can be considered as one of the main raw "materials" and corresponds to approximately 70% of the production cost [28]. The majority of the electricity is used in the electrolysis cells. The total energy consumption is in the range of 4.5-5.5 MWh/ton of sodium chlorate [29], of which approximately half is thermodynamically required for chlorate production and the rest leads to the low-value by-product of heat [27].

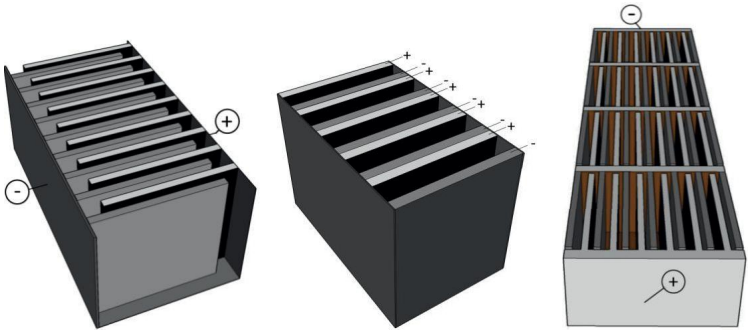

Figure 3 – Electrode configurations for chlorate production: a) monopolar, b) bipolar and c) multi-monopolar.

The operating conditions are carefully controlled and optimized to achieve the lowest overall production cost. Typical electrolyte compositions and operation parameters are listed in Table 1. In this process, a high chlorate concentration ensures efficient crystallization and allows dichromate and chlorides to be separated by their solubility differences. Chloride is the main reactant at the anode and hence needs to be added in excess. Furthermore, higher chloride concentrations improve the electrolyte conductivity, decreasing losses from internal resistances. However, the chloride concentration is limited to between 80 and 110 g dm^{-3} to avoid co-precipitation with chlorate in the crystallizer.

Table 1 – Electrolyte and cell parameters for chlorate production [1, 14, 30].

Operating conditions	
Chlorate (g dm^{-3})	450-630
Chloride (g dm^{-3})	80-110
Hypochlorite (ClO^- + HClO) (g dm^{-3})	Variable*
Sodium dichromate (g dm^{-3})	2-7
pH	5.8-6.5
Temperature (°C)	70-85
Current density (kA m^{-2})	~ 2-3
Current efficiency (%)	> 92-95
Cell potential (V)	2.8-3.3

* Hypochlorite is produced and consumed during the process (Section 2.2).

The pH varies along the whole process. The range presented in Table 1 refers to the optimum pH for chlorate formation in the reaction tank. The chlorate-forming reaction has the highest rate at pH 5.8-6.5, meaning that chlorate begins to form in the cells. In the cell gap (space between the cathode and anode), the pH varies from acidic to alkaline, moving from the anode to the cathode (Figure 4), because protons and hydroxides produced during the electrochemical reactions. The elevated temperature plays an important role in avoiding the crystallization of sodium chlorate, decreasing the cell potential and increasing the reaction rate.

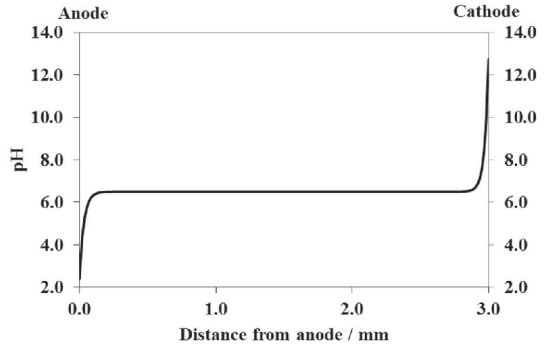

Figure 4 - Sketch of pH variation within a 3 mm electrode gap.

2.2. Electrochemical reactions in chlorate production

The main electrochemical reactions in the sodium chlorate process are water reduction (Equation 3) and chloride oxidation (Equation 4). Due to the production of gaseous H_2 and Cl_2, Equations 3 and 4 can be called the hydrogen evolution reaction (HER) and chlorine evolution reaction (CER), respectively. The standard potentials for the half-reaction are also presented in Equations 3 and 4.

$$2H_2O + 2e^- \rightarrow H_2 + 2OH^- \qquad E^o = -0.828 \text{ V vs. NHE (pH = 14)} \qquad (3)$$

$$2Cl^- \rightarrow Cl_2 + 2e^- \qquad E^o = +1.360 \text{ V vs. NHE} \qquad (4)$$

The HER is strongly dependent on the pH. The Nernst equation for the HER is given in Equation 5. At 25 °C, the thermodynamic potential for the HER varies by -0.059 V with each pH unit, reaching a maximum of -0.828 V at pH 14. The value of E^0 for proton reduction at pH 0 is the reference potential for all redox reactions and is arbitrarily defined as 0.0 V.

$$E = E^0 + \frac{RT}{nF}\ln\left[H^+\right]^2 = -0.059 \times pH \qquad (5)$$

where E^0 is the standard potential, R is the gas constant, T is the absolute temperature, n is the number of electrons and F is Faraday's constant. Hydroxide ions produced during the reduction of water (Equation 3) create an area of high pH in the vicinity of the cathode, even though the bulk pH is ~6.5. The actual pH at the cathode surface cannot be experimentally measured, but it can be as high as 14. Hence, the thermodynamic potential for water reduction is considered to be close to -0.826 V vs. NHE. At the anode, the CER leads to a decrease in the pH near the surface due to proton formation during chlorine hydrolysis (see Equation 6), explaining the pH profile in the electrode gap in Figure 4.

Under normal operating conditions, a commercial chlorate cell operates with a total cell voltage of 2.9-3.3 V. This value is the sum of all losses in the cell plus the thermodynamic potentials for alkaline water reduction and chloride oxidation. In Figure 5, a schematic presentation of all

contributions for the cell potential is shown. The anodic and cathodic overpotential[1] account for up to 700 mV, wherein 40-100 mV are from losses at the anode [31, 32] and 220-400 mV are from losses at the cathode [30, 33]. The low overpotential for the CER displayed by DSA gives very little room for improvement of the anode. However, efforts can still be made to lower the overpotential displayed by the cathodes. Unfortunately, suitable replacements for mild steel are limited by durability under the process conditions as well as process efficiency.

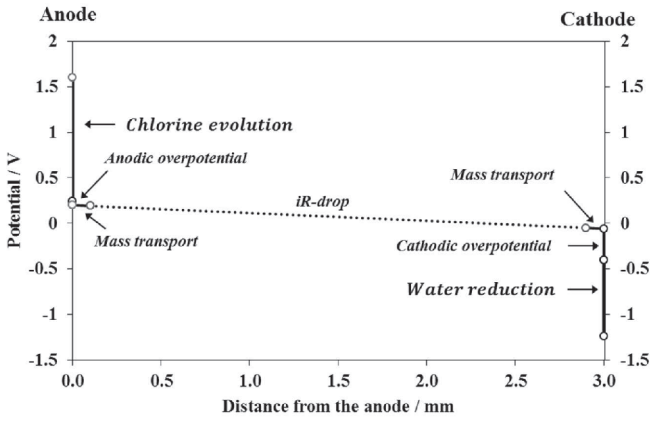

Figure 5 – Schematic representation of the cell potential distribution in the electrode gap [34].

In addition to the thermodynamic potential and the overpotential, a potential drop over the electrode gap occurs due to both the solution resistance (i.e. the iR-drop) and mass transfer. Together, they contribute roughly with 260 mV [33], most of which comes from the iR-drop. The potential drop in the gap can be lowered by increasing the electrolyte conductivity and/or decrease the gap dimensions. However, extensive redesign of the cells is required, which is beyond the scope of this thesis.

2.3.Chemical chlorate formation

The reaction mechanism leading to chlorate production was proposed by Foerster and Müller [18]. Anodic chlorine evolution (Equation 4) triggers a series of consecutive reactions in the bulk

[1] Overpotential is the excess potential compared to the thermodynamic potential calculated by the Nernst equation. Its magnitude is intrinsically dependent on the reaction kinetics.

of the electrolyte. The first reaction is the hydrolysis of chlorine, which forms hypochlorous acid and protons (Equation 6), causing the pH in the vicinity of the anode to decrease sharply (Figure 4). In water at 25 ºC [35], hypochlorous acid, which has a pKa of 7.53, will be in equilibrium with hypochlorite (Reaction 7) in the bulk, where the pH is no longer affected by chloride hydrolysis. Chlorate is formed by a disproportionation reaction between hypochlorous acid and hypochlorite (Equation 8).

$$Cl_2 + H_2O \leftrightarrow HClO + OH^- \quad (6)$$

$$HClO \leftrightarrow H^+ + ClO^- \qquad pK_a = 7.53 \quad (7)$$

$$2HClO + ClO^- \leftrightarrow ClO_3^- + 2Cl^- + 2H^+ \quad (8)$$

Equation 8 indicates that the highest reaction rate for chlorate formation occurs at the pH at which the HClO/ClO^- ratio is 2:1. This value is obtained at 0.3 pH units below the pKa, i.e., at pH 7.2, at room temperature in dilute solution. However, in the process, the high ionic strength and temperature may affect the equilibrium stabilization between hypochlorous acid and hypochlorite. Thus, the optimum pH for this process lies somewhere between 6.0 and 7.0.

2.4. Unwanted process reactions

Chlorate electrosynthesis is hampered by chemical or electrochemical reactions that decrease the production yield. These are called side, parasitic or unwanted reactions. These reactions cause severe losses in the process by decreasing the current efficiency. Current efficiency is defined as the amount of current that is converted to chlorate. The current efficiency is usually 90% or higher (Table 1), which means 90% of the current is used to reduce water and 10% is wasted on side reactions.

Another issue related to side reactions is the production of oxygen. Oxygen is an undesired reaction product in the cell gas, which mainly consists of hydrogen from the HER. If enough oxygen is produced, an explosive mixture H_2/O_2 can be formed. Therefore, the amount of oxygen in the cell gas is constantly analysed, and if it exceeds 3.0-3.5%, the plant is immediately shutdown. Such unscheduled shutdowns lead to severe production losses.

Unwanted anodic reactions leading to oxygen production are hypochlorous acid oxidation (Equations 9) and water oxidation (Equation 10). The oxidation of hypochlorous acid oxidation results also in chlorate formation, but this route is very inefficient. Other anodic side reaction is the oxidation of chlorate to perchlorate (Equation 11). These reactions, however, became of minor importance when DSA electrodes were introduced to the process. DSAs display higher overpotential for water oxidation and suppresses hypochlorite oxidation [31]. Chlorate oxidation has very slow kinetics and does not considerably affect the anodic current efficiency [31].

$$12HClO + 6H_2O \rightarrow 4ClO_3^- + 8Cl^- + 24H^+ + 3O_2 + 12e^- \quad (9)$$

$$2H_2O \rightarrow O_2 + 4H^+ + 4e^- \quad (10)$$

$$ClO_3^- + H_2O \rightarrow ClO_4^- + 2H^+ + 2e^- \quad (11)$$

Unwanted bulk (or chemical) reactions also contribute to increasing the O_2 level and decreasing the current efficiency. The most common reactions are hypochlorous acid and hypochlorite decomposition (Equations 12 and 13). To prevent these reactions, fast chlorate conversion must be ensured, and ions that catalyse hypochlorite decomposition must be kept at the lowest possible level.

$$2HClO \rightarrow 2HCl + O_2 \quad (12)$$

$$2ClO^- \rightarrow 2Cl^- + O_2 \quad (13)$$

Unwanted cathodic reactions are of great importance. Hypochlorite (Equation 14) and chlorate (Equation 15) reduction are thermodynamically favoured over water reduction and readily occur on steel electrodes [10]. These reactions are the main reason sodium dichromate must be added to chlorate electrolytes, as will be detailed in the next section.

$$ClO^- + H_2O + 2e^- \rightarrow Cl^- + 2OH^- \qquad E^o = +0.890 \text{ V vs NHE} \quad (14)$$

$$ClO_3^- + 3H_2O + 6e^- \rightarrow Cl^- + 6OH^- \qquad E^o = +1.180 \text{ V vs NHE} \quad (15)$$

2.5. Sodium dichromate

Up to this point, this thesis has introduced the technology, electrochemistry and shortcomings of the chlorate production process. However, one of the most important aspects is the use of Cr(VI) in the process. All commercial technologies for chlorate production depend on sodium dichromate [27] or Cr(III) salts [17] as additives. The main subject of this thesis is the effect and function of dichromate in the chlorate process, with a special focus on the cathode. Thus, this section will further explore chromium and its most industrially relevant compound, sodium dichromate.

2.5.1. A brief history of chromium

The discovery of the element chromium dates back to 1779, when it was found by the Frenchman L. N. Vauquelin in a Siberian mineral. Chromium was isolated from the mineral crocoite ($PbCrO_4$) by reduction with charcoal. The name chromium comes from the Greek χρομα (colour) due to the variety of colours it presents in different compounds. Chromium is estimated to account for 122 ppm of the Earth's crustal rocks, which is comparable, for instance, to chlorine. Chromium is a hundred times more abundant than other metals of its own group (Mo and W). The chemistry of chromium is vast due to its large number of oxidation states (II, III, IV, V and VI) and its ability to form stable oxides, such as CrO_3, Cr_2O_5, CrO_2, Cr_2O_3, and Cr_3O_8 [36]. The commercially most important Cr(VI) compound is sodium dichromate. This versatile compound is applied in the paint, ink, rubber and ceramics industries and is also used as a catalyst in organic chemistry processes [36]. In the sodium chlorate process, a small amount of sodium dichromate results in outstanding yields by providing selectivity to the cathodes. However, its role in the whole process goes beyond the electrode-electrolyte interface and reaches further into the bulk solution.

2.5.2. Sodium dichromate in the chlorate process

The benefits of adding $Na_2Cr_2O_7$ to the electrolyte have been noted previously in the literature [37-39] and were nicely compiled by Endrődi et al. [40]. The main effects are recognized as corrosion protection of the cathode, buffering of the electrolyte, homogeneous catalyst for chlorate formation, providing high current efficiency and providing selectivity to the cathode.

2.5.3. Corrosion protection

The corrosion protection provided by dichromate in the chlorate process was studied by Cornell et al. [9]. A more general approach was given by Clark and McCreery [41]. The reduction of Cr(VI) creates a passive layer on the electrode. The layer changes the Fe corrosion voltammogram, shrinking and shifting the peaks related to Fe corrosion [9]. This layer also prevents Fe oxidation by delaying oxygen reduction [41].

In the presence of strong oxidizing agents, such as hypochlorite, the Cr(III) layer is oxidized, forming soluble species of Cr(VI). In this process, dissolution of the film is believed to occur as soon as the current is switched off, due to the high oxidizing power of the electrolyte and the high temperature. However, this may not be accurate. Wullf and Cornell [15] determined that the cathodic current efficiency (CCE) is quickly recovered after shutdown in the presence of 6 g dm^{-3}. They attributed this effect to the formation of a long-lasting film, the lifetime of which increases with increasing dichromate concentration, as determined by in situ measurements of the film thickness [13]. In further process-related measurements, Hedenstedt et al. [42] showed that the Cr(III) film at the cathode is not immediately oxidized and dissolved after shutdown. They also found that the extent of corrosion after shutdown decreased when the dichromate concentration was increased from 1 to 7 g dm^{-3} [42].

In summary, the corrosion protection provided by the addition of sodium dichromate is related to the formation and dissolution of the protective Cr(III) film. Though this effect is small, it is important in increasing the lifetime of mild steel cathodes.

2.5.4. Soluble Cr(VI) oxides and the buffering effect

Chromium (VI) in aqueous solution forms several species that are in equilibrium, chromic acid (H_2CrO_4), hydrogen chromate ($HCrO_4^-$), chromate (CrO_4^{2-}) and dichromate ($Cr_2O_7^{2-}$), and the speciation depends on the pH and Cr(VI) concentration. In Figure 6, the speciation of Cr(VI) as a function of pH in a solution containing 5 mg dm^{-3} (40mM) is presented. The pKa values are given in Equations 16 and 17. Hydrogen chromate dimerizes to form the ion dichromate, as shown in Equation 18 [36]. At a concentration of 5 g dm^{-3}, soluble Cr(VI) oxide species, i.e., $HCrO_4^-$, CrO_4^{2-} and $Cr_2O_7^{2-}$, coexist in the bulk of the electrolyte (Figure 6). The acid-base

equilibrium is extremely important for this process, since it buffers the electrolyte in the optimum pH range, i.e., where the rate of the chlorate formation reaction is maximized. Near the electrodes, the pH is drastically changed (Figure 4). In the acidic environment near the anode, the dominating species are $HCrO_4^-$ and $Cr_2O_7^{2-}$. Close to the cathode, chromate is the dominating species due to the high pH (Figure 4).

$$H_2CrO_4 \leftrightarrow HCrO_4^- + H^+ \qquad pK_a = 1 \qquad (16)$$

$$HCrO_4^- \leftrightarrow CrO_4^{2-} + H^+ \qquad pK_a = 5.8\text{-}6.5 \qquad (17)$$

$$2HCrO_4^- \leftrightarrow Cr_2O_7^{2-} + H_2O \qquad K_c \sim 10^{-15} \qquad (18)$$

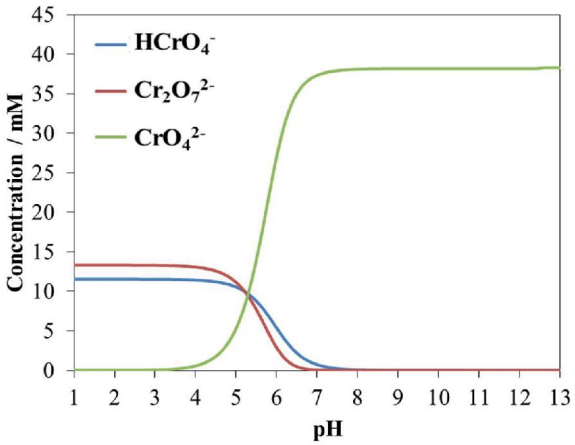

Figure 6 – Cr(VI) speciation in chlorate electrolyte when I = 6.4 M at 80 ℃.

2.5.5. Homogeneous catalyst for chlorate formation

Cr(VI) can also catalyse the chlorate formation reaction [38, 39, 43]. Chromate enhances the rate of chlorate formation, resulting in a decrease in the steady-state concentration of hypochlorite in the electrolyte [44]. A lower hypochlorite concentration in the electrolyte leads to fewer losses due to anodic (Equation 9), bulk (Equations 12 and 13) and cathodic (Equation 14) side reactions. Such effect has a large impact on the whole process and must be considered in any analysis of alternatives to the addition of dichromate.

2.5.6. Cathodic Cr(III) film formation

A cathodic Cr(III) oxide-like film is produced as a result of sodium dichromate reduction [9, 11-13, 16, 19, 45, 46]. Also known as a passive oxide layer [41, 47], the film formation occurs quickly in benchtop experiments [45] but can take longer on the industrial scale (based on CCE measurements and cell potential). Interestingly, the film provides selectivity to the cathodes, meaning that it inhibits hypochlorite and chlorate reduction, while allows water reduction to proceed with a marginal increase in overpotential [11, 12, 16, 19, 41, 46, 48]. The mechanisms by which the film provides selectivity, however, are still unclear. Müller was the first to propose film formation to explain the increase in current efficiency [48]. Sixty years after Müller's publication, Wagner was the first to propose a mechanism for the lack of cathodic hypochlorite reduction in the presence of the film [16]. With limited knowledge of the characteristics of the Cr(III) films, such as composition and thickness, Wagner believed that the film was porous and that electrostatic repulsions between an adverse potential gradient within the pores and negatively charged ions (such as hypochlorite and chlorate) could explain the hindrance mechanism.

Wagner's proposal, however, was challenged only one year later by Kolthoff and Shams El Din [19], who performed an extensive study on the electrochemical reduction of anions and cations on pre-formed Cr(III) films by the reduction of chromate. They showed that the film did not completely block the reduction of negatively charged ions such as permanganate and iodine. On the other hand, the reduction of cations such as Fe^{3+} and Cu^{2+} was completely blocked by the Cr(III) film. Thus, the adverse potential cannot fully explain the mechanism of the film.

After the study published by Kolthoff and Shams El Din [19], the selectivity provided by dichromate did not attract much attention in the scientific community [46] until a partnership between AkzoNobel (formerly, Eka Nobel AB), Permascand AB and the Royal Institute of Technology in Stockholm (Kungliga Tekniska Högskolan, KTH, Sweden) brought it back to the pages of peer reviewed journals [9, 11-13, 15, 22, 23, 45, 49]. The main motivation of this partnership was to understand in more detail the film structure [13], thickness [45], selective mechanisms [11, 12], effects of different cathode materials [9, 11, 12], effects on current efficiency [15] and possible replacements [22, 23, 49].

Lindbergh and Simonsson [11, 12] performed thorough experiments to electrochemically characterize the films formed during the electroreduction of chromate. Through their studies, the theory of an adverse potential gradient was once again refuted. They proposed, instead, the formation of a $Cr(OH)_3 \cdot xH_2O$ selective film that physically blocks the transport of hypochlorite to the electrode. According to their conclusions, the use of a porous diaphragm on the electrode surface would provide the same selectivity. This theory motivated several studies in which different hydroxide-forming cations were investigated. For example, the use of trivalent metal ions resulted in fairly selective electrodes in benchtop tests and dilute solutions [22, 23, 49]. However, the trivalent metal ions produced unsatisfactory results in long-term tests and presented incompatibilities with process electrolytes [22, 23, 49]. Sodium molybdate [24, 50] or the deposition of MoO_2 nanoparticles [25] also appeared as possible alternatives. The former, however, resulted in increased O_2 production [24, 50]. The latter was entrapped in a thick Cr_2O_3 film, and the effects of MoO_2 could not be isolated [25]. As of now, no replacement has been found [40].

Finding suitable replacements for dichromate goes beyond finding a good blocking system. The immediate challenge is to find a selective cathode. As previously mentioned, the Cr(III) film formed by chromate reduction avoids unwanted cathodic reactions but allows water reduction. The idea of a selective Cr(III) film physically hindering the transport of hypochlorite to the surface can be applied to Pt and Fe [9, 11, 12] or even RuO_2 [21] and Rh [51], where hypochlorite reduction was blocked and the HER occurred at higher overpotentials. The increase in overpotential was explained by reduced water transport through the Cr(III) film. However, a different result was obtained with Au electrodes [12]. In contrast to the results obtained using Pt and Fe electrodes, the HER was enhanced on Au electrodes in the presence of Cr(III) films. This led to the conclusion that the Cr(III) film has its own catalytic activity and cannot be seen simply as an inert barrier. Therefore, new mechanism combining the blocking effect and the catalytic activity towards HER is proposed in this thesis.

3. Methods and techniques

This chapter describes the experimental techniques used in this work for the electrochemical characterization of hypochlorite and water reduction, as well as for surface characterization of the electrodes.

3.1. Electrochemical methods

All electrochemical experiments in this thesis were performed using a three-electrode cell, as detailed in Figure 7a. Rotating disk electrodes (RDEs) (Figure 7b) were submerged in the electrolyte, and the rotation system was composed of an engine and a motor controller. The cell potential was measured against a Ag/AgCl reference electrode (Figure 7c) coupled to a glass double-junction filled with electrolyte. The inner electrolyte in the reference electrode was either 3 M KCl (+0.210 vs. SHE) or saturated NaCl solution (+0.197 vs SHE). The counter electrode

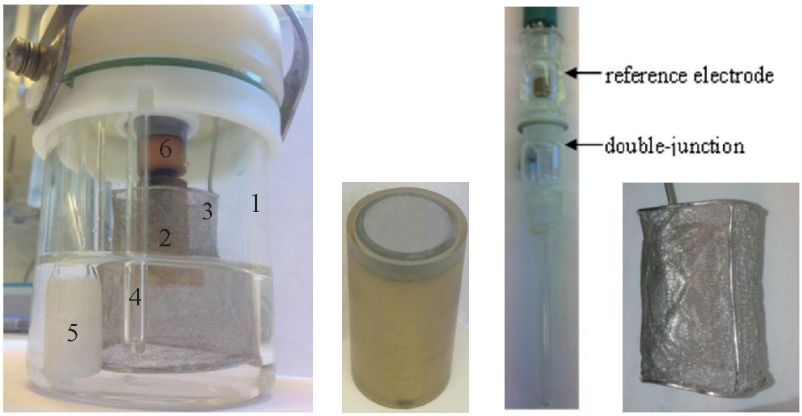

Figure 7 – a) Three-electrode cell set up used for the electrochemical experiments: 1 – cell made of glass, 2 – working rotating disk electrode (inside the counter electrode), 3 – round platinum mesh as the counter electrode, 4 – double-junction filled with electrolyte, 5 – sintered glass gas distribution tube for the nitrogen inlet, 6 – rotator and electric contact. Photographs of the b) rotating disk electrode, c) double-junction and Ag/AgCl electrode and d) counter electrode.

(Figure 7d) was a platinum mesh with high surface area surrounding the working electrode. N_2 purging was performed by forcing pure nitrogen gas through a porous glass tube or simply through a Pasteur pipet.

The RDE configuration is common in electrochemistry. The hydrodynamic flow towards the electrode is well defined (Figure 8) and provides a steady-state condition at its surface, in which fresh electrolyte is always fed and reaction products are always removed by the centrifugal force. Mass transfer to the RDE was solved by the Russian mathematician Levich [52].

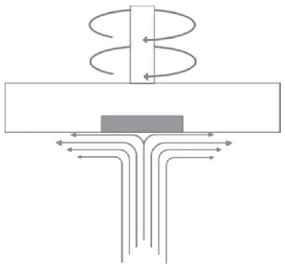

Figure 8 –Side view of the electrolyte flux using a rotating disk electrode.

3.2. Cyclic and linear sweep voltammetry

Cyclic voltammetry (CV) and linear sweep voltammetry (LSV) are two of the most applied techniques in electrochemistry to study redox reactions. In both techniques, the electrode potential is varied at a constant rate over time. In CV, the potential scan goes from the starting potential to the switching potential and back to the starting potential (Figure 9a). In LSV, the potential sweep goes only in one direction, stopping at a set potential limit (Figure 9b). The current is measured as a function of potential, and the plot of I vs. E is called a voltammogram.

Kinetics and mass-transfer limitations

The steady-state regime of mass transfer is assumed when RDE configuration and a slow sweep rates are used. In this case, if the rate of electron transfer is fast, the entire curve depends on mass transfer, and the Nernst equation holds. The current is limited by the flux of species to the surface, and a limiting current appears when the concentration of the electroactive species

becomes zero at the surface (Figure 9c). This mass-transfer limiting current appears as a plateau in the voltammogram (Figure 9c) and can be calculated by the Levich equation (Equation 19),

$$I_{\text{lim}} = 0.62nFAD_0^{2/3}\nu^{-1/6}\omega^{1/2}C^* \tag{19}$$

where n is the number of electrons, F is Faraday's constant, A is the electrode geometrical area, D_o is the diffusion coefficient, ν is the kinematic viscosity, ω is the rotation rate and C* is the bulk concentration of reactant in solution. In the case of irreversible electron transfer, currents are limited by charge transfer at low overpotentials and by mass transfer at sufficiently high overpotentials (Figure 9c). The total current can be divided into two terms depending on the kinetics of electron transfer and mass transfer, as shown in Equation 20. The equation is commonly known as the Koutecký-Levich equation [53].

$$\frac{1}{I_{tot}} = \frac{1}{I_k} + \frac{1}{I_{\text{lim}}} = \frac{1}{I_k} + \frac{1}{0.62nFAD_0^{2/3}\omega^{1/2}\nu^{-1/6}C^*} \tag{20}$$

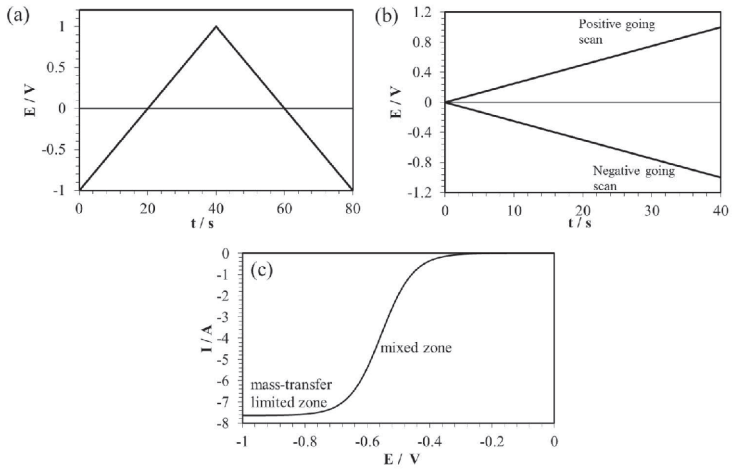

Figure 9 – Potential variation as a function of time in a) cyclic voltammetry and b) linear sweep voltammetry. In (a) and (b), the potential limits are set to +1.0 and -1.0 V. c) Current (I) measured as a function of potential (E) using linear sweep voltammetry and the RDE configuration.

The kinetic current in the Koutecký-Levich relationship can be obtained from the Butler-Volmer equation (Equation 21). For a reduction reaction involving irreversible one-step one-electron transfer (such as H_2 evolution), the reverse reaction (H_2 oxidation) is limited by very slow electron transfer, and the anodic term of the Butler-Volmer equation (second term on the right side) is negligible.

$$I = I_0\left[\exp\left(\frac{-\alpha nF(E-E^0)}{RT}\right) - \exp\left(\frac{(1-\alpha)nF(E-E^0)}{RT}\right)\right] \quad (21)$$

where I_0 is the exchange current density, α is the charge-transfer coefficient, R is the gas constant, T is the absolute temperature, η is the overpotential and k is the electrochemical rate constant. Equation 21 can be used to fit the experimental data in the voltammogram, allowing the precise calculation of the charge-transfer coefficient and electrochemical rate constant.

The charge-transfer coefficient, α, is a symmetric factor that expresses the structure of the activated complex. The activated complex is a transient state of molecules during a chemical or electrochemical reaction. α can be easily obtained from the voltammogram, which gives a slope *b*, as presented in Equations 22a and 22b. The value of α is assumed to be 0.5 for symmetrical reactions, meaning that the activated complex assumes a structure equally similar to the reactants and products. The Tafel slope in this case is 120 mV dec^{-1}. In Equations 22a and 22b, the cathodic and anodic equations are related to the reduction and oxidation Tafel slopes, respectively.

$$\frac{1}{b} = -\frac{\ln(10)RT}{\alpha nF} \text{ (cathodic Tafel slope)} \quad (22a)$$

$$\frac{1}{b} = \frac{\ln(10)RT}{(1-\alpha)nF} \text{ (anodic Tafel slope)} \quad (22b)$$

Capacitance measurements using CV

In addition to the faradaic current described above, contributions from capacitive currents can also be seen in a voltammogram. In the potential region at which no electrochemical reaction occurs, currents can still differ from zero due to electrochemical double-layer charging. The electrochemical double layer can be seen as a parallel-plate capacitor, where one of the "plates"

is the electrode surface and the other is formed by ions in solution. When a potential is applied in the electrode, ions of opposite charge in the solution are attracted to the electrode, forming a densely packed structure in the vicinity of the electrode surface. This phenomenon is known as double-layer charging, and the currents associated with this process are called capacitive currents. The capacitive currents can be calculated using Equation 23 [54]. For flat, polished metal electrodes, the capacitance is on the order of 20 μF cm^{-2} and is negligible at low sweep rates [54]. Large capacitive currents, which are obtained for porous metal oxides with large surface area, affect the voltammogram and must be subtracted for precise catalytic analyses.

$$I_d = \nu C_d \left[1 - \exp\left(\frac{t}{C_d R_s} \right) \right] \quad (23)$$

where I_d is the capacitive current, ν is the sweep rate, C_d is the double-layer capacitance, t is the time and R_s is the solution resistance.

3.3. Steady-state polarization

In potentiodynamic techniques (CV or LSV), the effects of double-layer charging may affect the precise calculation of kinetic and mass-transfer parameters. As an alternative to potential sweep techniques, steady-state polarization can be used. In steady-state polarization, constant potentials are applied for longer periods of time (tenths of seconds to hours), and the current is measured as a function of time. During steady-state polarization, the effects of capacitance vanish, and electron transfer is the only process occurring in the kinetic zone. However, mass-transfer limitations are still observed at sufficiently high overpotential. The current response is called the steady-state current, I_{ss}, or i_{ss} if the steady-state current density is used instead (where $i_{ss} = I_{ss}/A$). By applying different steady-state potentials, the curve of I_{ss} vs. E can be plotted, and the electrode kinetics can be evaluated free of the double-layer charging contribution (this was done in Paper 2, where kinetic currents for HER were evaluated on Cr(III) films deposited on Ti electrodes).

3.4. Electrochemical impedance spectroscopy

Electrochemical impedance spectroscopy (EIS) is a very powerful technique that can give information on the rate constants, diffusion coefficients, double-layer capacitance, exchange current, etc. In EIS, the electrochemical cell is seen as an electric circuit, and the various components (resistances, capacitors, inductors, etc.) describe electrochemical processes, such as solution resistance, electron-transfer resistance, and double-layer capacitance. EIS measurements are performed by applying a sigmoid (waveform) potential to a system near steady state. The frequency of the applied potential varies from high (100 kHz) to low (10 mHz), and the current response is logged. As Ohm's law holds, the impedance (Z) can be expressed as in Equation 24, where $\dot{E}$ and $\dot{I}$ are the potential and current, respectively, written in phasor notation.

$$\dot{E} = \dot{I}Z \tag{24}$$

Z is the sum of all voltage drops across the circuit and is dependent on the frequency of the perturbation signal. Z can simply be represented as in Equation 25, where Z' is the "real" impedance and Z" is the "imaginary" impedance. The real part, Z', expresses pure resistances, while the imaginary part, Z", carries information on voltage drops across the capacitors. j is the complex number $\sqrt{-1}$ and indicates components in the ordinate axis.

$$Z(\omega) = Z' - jZ'' \tag{25}$$

From Z', two important parameters are obtained. At high frequencies, the impedance corresponds to the solution resistance, R_0, that can mathematically compensate for I vs. E measurements in the case of non-transient techniques, such as those obtained with RDEs. At low frequencies, the charge-transfer resistance, or R_{ct}, is found. As R_{ct} decreases with increasing potential, "pseudo-Tafel plots" can be obtained by plotting $\log(1/R_{ct})$ vs. E [55]. This method was used in this thesis to compare "pseudo-Tafel slopes" from EIS with Tafel slopes from I_{ss} measurements.

3.5. Surface characterization techniques

Electrochemical processes are intimately connected to the composition and morphology of electrodes. Hence, the results obtained electrochemically can only be well evaluated if the electrode material is very well characterized before (and sometimes after) the experiments. The complete characterization of an electrode is usually complex, since the information lies on the micro- or nanoscale. Therefore, multiple characterization techniques are necessary. In this thesis, for example, the electrodes were characterized using scanning electron microscopy (SEM), energy dispersive x-ray spectroscopy (EDX), x-ray diffraction (XRD), x-ray photoelectron spectroscopy (XPS) and Raman spectroscopy, which will be described in some detail.

3.5.1. Scanning electron microscopy (SEM)

SEM is an advanced technique to study the morphology of the electrode surface using an electron beam. The wavelength of an electron is shorter than that of visible light and is not limited by Snell's law of resolution [56]. Hence, in SEM, high-resolution images with high magnifications (up to 1,000,000×) can be obtained.

The electron beam is formed by a thermionic gun (W, LaB_6) or a more advanced field-emission gun (FEG). The beam goes through a set of magnetic lenses before hitting the sample. Electrons are scattered back and detected in an Everhart-Thornley (ET) detector. The surface is scanned in a raster fashion.

In this process, electrons can be inelastically (secondary electrons, SE) or elastically (backscattered electrons, BSE) scattered. The energy differences between SE and BSE allow them to be detected separately. Secondary electrons come from the outermost layers and carry information on the morphology. They have a good signal-to-noise ratio, and allow a resolution down to 1 nm as well as 3D observation of the surface. Backscattered electrons arise from deeper portions of the sample. The signal-to-noise ratio of BSE is low, and no 3D information is obtained. In BSE mode, however, the position of different elements on the surface can be observed, since the recorded signal is proportional to the atomic number (hence, heavy elements appear brighter). Still, elements cannot be identified using SEM only, and X-ray-based techniques are required for a complete investigation of the sample.

3.5.2. Energy dispersive X-ray spectroscopy (EDX)

EDX (or EDS) is a qualitative or semi-quantitative technique to investigate the surface composition. EDX is usually coupled with SEM, and the analysis can focus on a specific point or on a larger portion of the surface.

In EDX, a high-energy electron beam is irradiated on the sample, knocking out electrons from the K-shell. The voids are fulfilled with electrons that decay from more-energetic shells (L or M) with the emission of X-rays. The energy of the emitted photon is proportional to the atomic number and, therefore, is specific to each element.

The EDX resolution is limited by the interaction volume generated by electrons that penetrate deep (a couple of μm) into the sample. The interaction volume has the shape of a pear and is proportional to the energy of the electron beam, the sample composition and the density. It is difficult to obtain the size of the interaction volume, but its effects can be mitigated by using lower beam energies, when possible.

3.5.3. X-ray diffraction (XRD)

X-ray diffraction is a technique to characterize the composition of a solid crystalline material. XRD is a more surface-sensitive and complete characterization technique than, for instance, EDX. In XRD, X-rays are irradiated to and reflected from the *lattices* of a crystalline solid (Figure 10). Detailed information about the crystal and molecular structure of the sample is revealed by the reflections that result from constructive interferences between X-rays scattered in parallel lattices, described by Bragg's law (Equation 26).

$$n\lambda = 2d\sin\theta \quad (26)$$

where n is an integer, λ is the wavelength, θ is the angle of incidence and reflection, and d is the distance between lattices, which is unique for each crystal, resulting in unmistakable diffraction patterns.

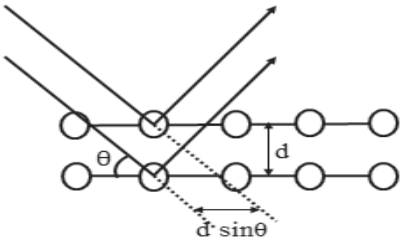

Figure 10 – Simplified Bragg's lattice schematic.

To achieve well-resolved diffractograms for polycrystalline samples, the faces of a crystalline solid must be randomly oriented; otherwise, some reflections may be absent, and others may be more prominent. In this case, the solid is said to have a preferred orientation. When a sample presents a preferred orientation, its analysis is more difficult but not impossible.

XRD not only reveals the crystalline structure of the solid but also allows the estimation of the particle size if the material is a powder. This is done by applying Equation 27, which is known as Scherrer's equation [57]. In this equation, the particle size (D) obtained from the diffractogram is inversely proportional to peak broadening (β)[2]. The other parameters included in the equation are the wavelength (λ = 1.5418 nm for Cu K_α) and the Bragg's angle (θ). K is a dimensionless shape factor, assumed to be 0.89 in this work.

$$D = \frac{K\lambda}{\beta\cos(\theta)} \tag{27}$$

Some materials are completely "invisible" in XRD, meaning no single reflection is observed. This is caused by the total lack of periodicity in the solid structure, even if the composition is homogeneous, and such material is called XRD amorphous (Greek word for formless). To determine the molecular structure of amorphous materials, other techniques are necessary.

[2] β is the full width at half maximum of the peak.

3.5.4. X-ray photoelectron spectroscopy (XPS)

X-ray photoelectron spectroscopy (XPS) is a technique to study the outermost layers of a surface using a high-energy X-ray source. XPS has the advantage of identifying and quantifying (in %) different molecules of a XRD crystalline or amorphous sample. The technique reveals the elemental composition and gives the empirical formula as well as the chemical and electronic states of the elements composing the material. Therefore, XPS is also called "electron spectroscopy for chemical analysis" (ESCA). In contrast to XRD or EDX, XPS is based on the photoionization phenomenon, which relates to electrons in the valence shell. An XPS spectrum is constructed by plotting the number of electrons (counts) versus their binding energy (in eV).

The number of electrons expelled from the surface is directly dependent on the atomic number, oxidation state and chemical environment, i.e., the chemical bonds in the solid. Detection is achieved by an electron energy analyser, which simultaneously counts the number of expelled electrons and resolves their kinetic energy (E_k). E_k (Equation 28) is a function of the X-ray energy ($h\nu$) and the binding energy (E_B) of the electron, which is dependent on the chemical bond. The work function (E_w) is also considered, since E_B is conveniently measured with respect to the Fermi-level of the solid.

$$E_K = h\nu - E_B - E_w \qquad (28)$$

where h is Planck's constant and ν is the irradiation frequency.

XPS is not a direct technique like XRD or EDX, and the data need to be properly evaluated to obtain meaningful results. An internal standard is required to correct the positioning of the peaks. The most common internal standard is carbon (^{12}C), which is usually present as a contaminant. The peak for ^{12}C is positioned at 285.5 eV, and all other peaks are shifted according to the carbon peak.

3.5.5. Raman spectroscopy

In Raman spectroscopy the vibrational, translational and rotational modes of a molecule are studied by irradiating the sample with a laser (in the visible-light range). Photons that interact with the sample are scattered and detected perpendicular to the irradiation path. The results are

plotted as the number of photons counted as a function of the wavelength (cm^{-1}), which is called Raman spectrum.

When light is irradiated on a sample, it interacts with the molecules, exciting them to a virtual excited state that lies below the first excited electronic state. Relaxation to lower energy levels occurs with the emission of a photon (Figure 11). Most of the scattered photons are elastically irradiated (Rayleigh effect), meaning that they have the same energy and wavelength as the incident photon. Rarely (a 1×10^{-6} chance), the photon emission is inelastic, and this phenomenon is called the Raman effect. The inelastic scattering can be of lower (Stokes) or higher (anti-Stokes) energy than the incident photon (Figure 11). As molecules are commonly at their lowest energy state, the Stokes process is more common and appears with greater intensity in the Raman spectrum [58].

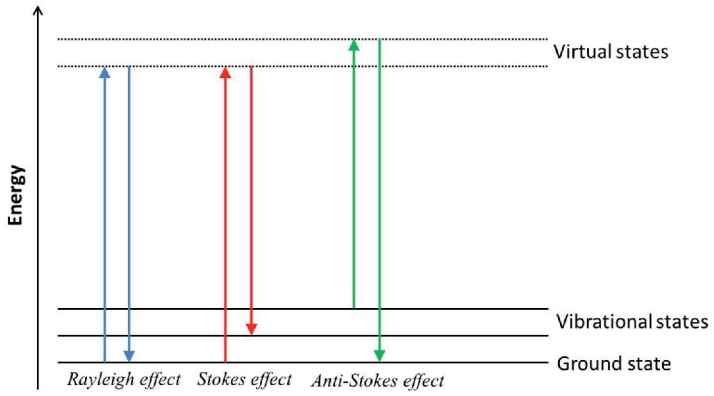

Figure 11 – Schematic presentation of the excitation (arrows pointing up) and relaxation (arrows pointing down) of a molecule under irradiation.

Not all molecules or molecular vibrations are active in Raman spectroscopy. To be active, the derivative of the polarizability, α, with respect to the vibration amplitude, Q, has to be different from zero [59]. The intensity, I_R, of a Raman peak is given in Equation (29), where it can be immediately seen that if $\left(\partial\alpha/\partial Q\right) = 0$, the particular molecular vibration is absent from the Raman spectrum.

$$I_R \propto \nu^4 I_0 N \left(\frac{\partial \alpha}{\partial Q} \right)^2 \quad (29)$$

where ν and I_0 are the frequency and intensity of the incident laser, respectively, and N is the number of scattering molecules in a given state.

The Raman spectrum is specific for each molecule and can be used to identify the composition of $Cr(OH)_3$ and Cr_2O_3 films deposited on electrodes. Additionally, Raman spectroscopy can be used to determine the structure of $Cr(OH)_3$ and Cr_2O_3 nanoparticles (Paper 5).

3.5.6. Thermogravimetric analysis and differential scanning calorimetry

Analysis of the mass (m) loss as a function of time (dm/dt) and temperature (dm/dT) is called thermogravimetric analysis (TGA). This is a simple technique to analyse the degree of hydration of a crystal, the stability of a material (as a function of T), the amount of organic matter in soil, etc. [60]. This technique consists of weighing a certain amount of sample – usually a few milligrams is enough – placed on a cantilever using a very-high-precision microbalance (1 µg precision) positioned inside the equipment. The chamber is sealed, allowing rigorous control of the atmosphere. The initial mass is measured, and its variation as a function of time and temperature is recorded. Mass loss can occur in a single sharp drop, a single steady decay or in several steps, depending on the characteristics and composition of the sample and the temperature variation rate (dT/dt). Commonly, mass losses are related to the evaporation of water or organic solvents, the oxidation of organic compounds (due to CO/CO_2 release), the loss of volatile compounds (at a determined T), etc. In contrast, a mass increase in TGA can indicate, for instance, oxidation of a sample with the incorporation of O_2, which is one reason the atmosphere has to be carefully controlled; otherwise, the interpretation of data can be difficult [60].

TGA, however, is limited to the analysis of samples in which the mass changes as a function of temperature (or time). Several other temperature-induced transformations that do not involve any changes in mass can occur. For example, several compounds undergo conformational transitions upon heating. Crystallization can occur, or crystals can be destroyed without any mass change. Even the most obvious effect of melting is unnoticeable by TGA [61]. Hence, heat is also

analysed during a temperature scan. Analysis of the heat (Q) change over time (dQ/dt) and temperature (dQ/dT) is called differential scanning calorimetry (DSC).

Combining TGA and DSC, all transformations under a temperature increase/decrease can be monitored and rationalized, allowing the identification of the composition and stoichiometry of a sample. Addition information and technical aspects of TGA can be found in [60], and those for DSC in [61].

3.5.7. Electrode preparation

Ex situ $Cr(OH)_3$ and Cr_2O_3 films were prepared by electrodeposition using the potentiostatic technique. In this thesis, "ex situ" refers to Cr(III) films prepared in advance of the electrochemical measurement of chlorate-related reactions. This is opposed to the case of many other studies [9, 11, 12, 14-16, 18, 19, 46, 50], where dichromate was added to the electrolyte and the Cr(III) film was formed in situ.

The method involved the electrodeposition of pure phases of $Cr(OH)_3$ and Cr_2O_3 from two different CrO_3-rich solutions, presented in Table 2 [62]. The electrocatalytic properties, as well as the surface characteristics, of the different oxides could be studied prior to their examining behaviour in chlorate-related electrochemical reactions. Cr(III) films were coated on titanium (Ti), iron (Fe), gold (Au) RDEs. Ti and Fe were selected due to their process relevance; Au was used because of its widely known electrochemical properties and high catalytic activity towards hypochlorite reduction.

Table 2 – Electrolyte composition for the electrochemical deposition of Cr(III) species [62].

	$Cr(OH)_3$	**Cr_2O_3**
CrO_3 (g/L)	364	364
$BaCO_3$ (g/L)	9.1	9.1
H_2SiF_6 (g/L)	-	1.8
KNO_3 (g/L)	-	2.3

4. Ex situ electrodeposition and surface characterization

The characteristics of surfaces are extremely important when evaluating their electrochemical properties, since they are all strictly dependent on the surface composition and morphology. However, characterization is not always straightforward, not even on surfaces made ex situ.

This chapter will describe:

- the approach taken in this research to create well-defined surfaces
- the surface characterization of electrodes prepared for the electrochemical evaluation
- a critical insight in Raman spectroscopy for chromium oxides/hydroxides.

4.1. Ex situ electrodeposition: a new approach for an old problem

The approach in this thesis has been to start from well-defined ex situ-created surfaces, in order to correlate electrochemical data with the composition and structure of the films. In contrast, most papers on this topic do not report surface characterizations, focusing only on the selectivity provided by $Cr_2O_7^{2-}$ in the chlorate process [9, 11, 12, 16, 19, 63]. Attempts to characterize Cr(III) films formed from the reduction of $Cr_2O_7^{2-}$ appeared in different papers [13, 45, 64, 65]. However, the published results did not always agree, and the film could be defined as either $Cr(OH)_3$ [13, 45] or Cr_2O_3 [64] in pure or hydrated forms.

Despite 110 years of the use of sodium dichromate in the chlorate process, the actual molecular structure of the in situ-formed Cr(III) films is still an issue of debate. Complications arise from the extreme thin film formed (tenths of nanometres [45]) and possible structural changes due to film dehydration in air prior to ex situ analyses. The $Cr(OH)_3.xH_2O$ structure has been widely accepted even when $Cr_2O_3/Cr(OH)_3$ may have coexisted in the structure [9].

To overcome this limitation, $Cr(OH)_3$ and Cr_2O_3 films were produced ex situ, enabling the use of several surface characterization techniques prior to electrochemical investigations. By stablishing the films structure, the electrochemical behaviour of these films could be evaluated and compared with electrochemical data from in situ-formed films already discussed in the literature [9, 11, 12].

4.2. Surface characterization

The electrodeposition of pure $Cr(OH)_3$ and Cr_2O_3 phases was performed using a potentiostatic technique. The deposition electrolytes were proposed by Aguilar et al. [62] (see Section 3.6), and the resulting Cr coverages exhibited differences observable with the naked eye (Figure 12). The $Cr(OH)_3$ layer is presented in Figure 12a and displays a smooth white/greyish layer. In contrast, Figure 12b shows that Cr_2O_3 yields a thick black layer. These results are in agreement with literature [62, 66], where XPS was used to confirm the presence of $Cr(OH)_3$ and Cr_2O_3.

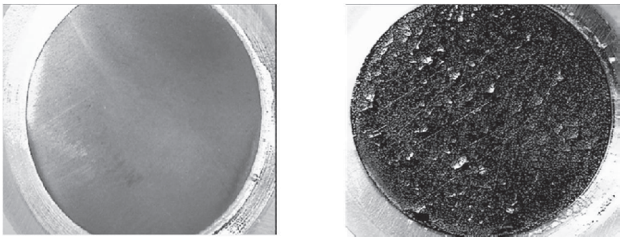

(a) (b)

Figure 12 – Titanium electrodes after $Cr(OH)_3$ (a) and Cr_2O_3 (b) electrodepositions.

4.2.1. SEM/EDX

Morphological analyses of the Cr(III) deposits were carried out using SEM. In Figure 13a, the $Cr(OH)_3$ film appears as a rough, unstructured surface. SEM images of the Cr_2O_3 deposit (Figure 13b) show that the electrode surface was homogeneously covered by plate-like crystallites, with sizes ranging from 500 to 1000 nm. These results are in good agreement with previous publications using the same electrodeposition baths [62, 66]. The atomic composition of the layers was obtained with EDX (Table 3). The $Cr(OH)_3$ film presented 20at% Cr and 55at% O. The ratio between Cr and O yields a value close to 1:3, as expected for $Cr(OH)_3$. Compositional analysis of Cr_2O_3 revealed 34at% Cr and 55at% O, with a Cr:O ratio close to 2:3. EDX gives no definitive proof of molecular structures, but it can be used as a strong indicator.

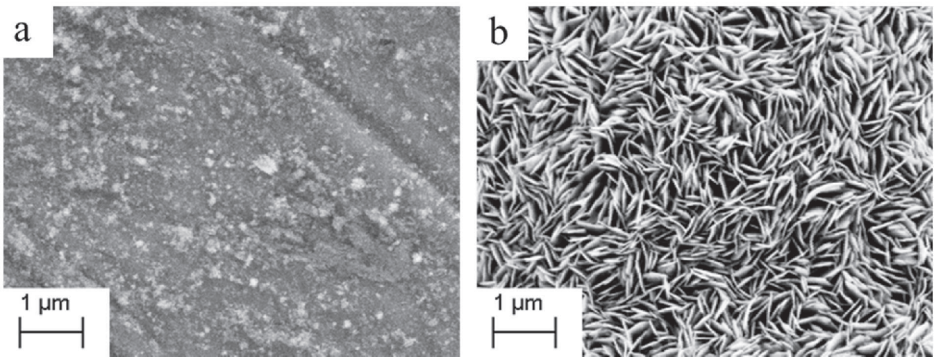

Figure 13 – Scanning electron microscopy (SEM) images of a) $Cr(OH)_3$- and b) Cr_2O_3-covered Ti electrodes, at 15000× magnification (Paper 2).

EDX is not suitable for determining film thicknesses due to the size of its interaction volume (Section 3.5.2). However, at the same electron acceleration, the interaction volume should be the same for surfaces with similar compositions. Signals arising from the substrate (Ti, in this case) can thus be used as a qualitative measurement of film thickness. Table 3 shows that the amount of Ti on the electrode covered with Cr_2O_3 is approximately 2%, compared to the 17% Ti detected in the $Cr(OH)_3$ film. Hence, the Cr_2O_3 layer is thus thicker than the $Cr(OH)_3$ film.

Table 3 – Compositional analysis using EDX of Ti electrodes covered with electrodeposited $Cr(OH)_3$ and Cr_2O_3 (Paper 2).

Surface	Cr (at%)	O (at%)	Ti (at%)
Cr_2O_3	37±5	47±10	2±1
$Cr(OH)_3$	20±1	55±8	17±7

4.2.2. XRD and XPS analyses

Since EDX gives a qualitative analysis of the film composition, XRD was used to confirm the film structure. The diffractograms recorded for $Cr(OH)_3$, however, did not show any evidence of crystalline phases related to Cr compounds (Paper 2, SI), revealing the amorphous character of the deposit [67-72]. Surprisingly, Cr_2O_3 deposits prepared by the method employed (Section 3.7) also resulted in an XRD amorphous film (Paper 2, SI). Cr_2O_3 is usually indicated to be crystalline

by XRD measurements [69-75], but a few references show diffractograms where Cr_2O_3 appears amorphous [62, 66, 76].

In the context of "black chromium" electrodeposition, XPS was used to determine surface composition of the deposits [62, 66, 76-78]. Black chromium was composed of a complex Cr(III) oxide matrix [62, 66, 79], and the material appears amorphous in XRD due to the lack of the long-range periodicity of crystallites that is necessary to fulfil Bragg's law (Section 3.5.3).

XPS was also applied in this work to determine the molecular structure of the $Cr(OH)_3$ and Cr_2O_3 films covering Ti electrodes. As stated in Section 3.5.4, XPS signals must be adjusted relative to a reference peak (usually C1s). However, the C1s reference peak could not be precisely positioned in this study (Paper 2, SI). A precise analysis of the deposited layers was thus compromised, and no phase identification was possible because the proximity of the binding energies of $Cr(OH)_3$ and Cr_2O_3. Still, XPS data (Paper 2, SI) have shown that the surfaces present a Cr(III) oxide-like structure and that the Cr_2O_3 layer is composed of a rather complex oxide matrix.

4.2.3. Raman spectroscopy

Raman spectroscopy was used as an alternative to XRD and XPS for the identification of the different electrodeposited $Cr(OH)_3$ and Cr_2O_3 films. The spectra were collected at different laser energies (from low to high) because the films absorbed light. The collected data are summarized in Figure 14.

Raman spectra from the electrode covered with $Cr(OH)_3$ are presented in Figure 14a. At the lowest laser energies (0.35 and 0.70 mW), only a weak Raman signature, at 850 cm^{-1}, was observed. At higher laser energies, a peak close to 550 cm^{-1} emerged, while the peak at 850 cm^{-1} diminished. At the highest laser energy, four distinct peaks, at approximately 610, 550, 350 and 310 cm^{-1}, typical for α–Cr_2O_3 [64, 71, 80-84] appeared, and the signature at 850 cm^{-1} completely vanished. The Raman spectra of Cr_2O_3 electrodeposited on Ti (Figure 14b) also showed no Raman signatures at the lowest laser power. However, peaks characteristic for α–Cr_2O_3 were observed at higher laser powers, similar to the hydroxide phase.

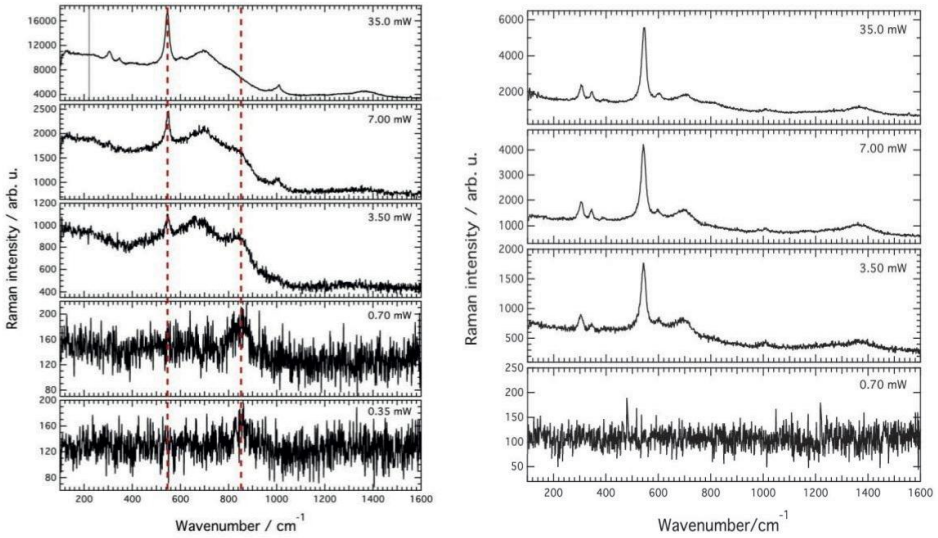

(a) (b)

Figure 14 – Raman spectra at several laser powers taken from Ti covered with a) $Cr(OH)_3$ film and b) Cr_2O_3 film (Paper 2).

Good reference data were needed for a correct interpretation of the Raman spectra of the films (Figure 14), and an extensive study on $Cr(OH)_3$ and Cr_3O_2 nanoparticles was done. $Cr(OH)_3$ and Cr_2O_3 nanoparticles were synthetized following the method given by Xu et al. [73]. In their method, $Cr(OH)_3$ was prepared by the hydrothermal method, and Cr_2O_3 was obtained after the calcination of $Cr(OH)_3$ at 900 ºC for 1 h. The resulting material was analysed by SEM/EDX, revealing nanoparticles with a wide size distribution and high purity (Paper 5). XRD analyses before and after calcination revealed that the proposed method was successful in producing amorphous $Cr(OH)_3$ and crystalline α-Cr_2O_3 (PDF 00-006-0504) nanoparticles (Paper 5). Due to its amorphous characteristics in XRD, the identification of the $Cr(OH)_3$ was accomplished with Raman spectroscopy.

Raman spectra of the $Cr(OH)_3$ and Cr_2O_3 nanoparticles are shown in Figure 15. The excitation source was the 532 nm line of a diode laser, and the laser power was 0.7 mW, corresponding to 1% of the maximum laser power (same as used for analysing the surfaces). The crystalline Cr_2O_3 was easily identified by the four characteristic peaks (Table 4) previously discussed in the

literature [64, 71, 80-84]. Contrarily, $Cr(OH)_3$ presented only two Raman broad features and has been rarely studied by Raman spectroscopy [85]. The identification of the $Cr(OH)_3$ phase was only possible by deconvolution of the signals (Paper 5, SI). A peak fit analysis was carried out and showed that six vibrational modes can perfectly fit the experimentally recorded Raman spectrum (Paper 5, SI), in agreement with the predictions given by Nielsen et al. [86]. The peak centred at 850 cm^{-1} was thus assigned to symmetric and anti-symmetric Cr–OH stretching, and the broad peak at 530 cm^{-1} was assigned to Cr–O–H bending modes.

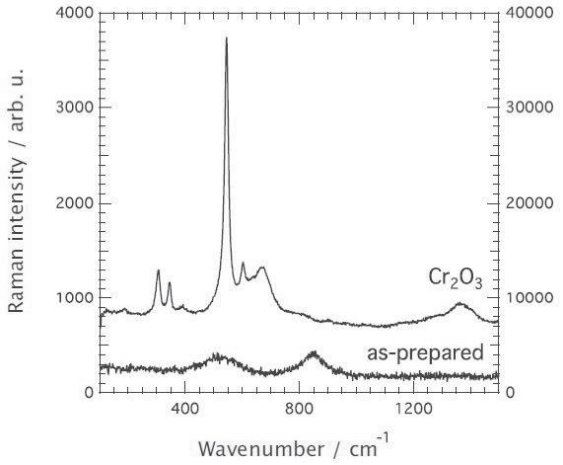

Figure 15 – Raman spectra from as-prepared ($Cr(OH)_3$) and calcined (α-Cr_2O_3), recorded at room temperature, using the 532 nm laser line and 0.7 mW laser power (Paper 5).

The results obtained for the nanoparticles, presented in Figure 15, were used to interpret the low-energy spectra collected for the films, given in Figure 14. The $Cr(OH)_3$ films presented a weak Raman signature at 850 cm^{-1} (Figure 14a), which matches well with the energies of the stretching modes of $Cr(OH)_3$ nanoparticles observed in Figure 15. The concordance between results is a strong indication that the deposition technique succeeded in producing a $Cr(OH)_3$ film.

In the case of the Cr_2O_3 deposit (Figure 14b), the low laser energy spectrum did not show any Raman signatures, oppose to data collected for the Cr_2O_3 nanoparticles (Figure 15). However, the films revealed to be XRD amorphous and composed of a complex Cr(III) oxide matrix

(Paper 2, SI). In contrast, the Cr_2O_3 nanoparticles were highly crystalline in XRD (Paper 5). So, Cr_2O_3 films and nanoparticles cannot be directly correlated. Still, the Cr_2O_3 films did not show any Raman signatures related to the hydroxides, and therefore were identified as an oxide.

Table 4 – Experimentally observed and theoretically calculated Raman-active modes for α-Cr_2O_3. *Observed only at low temperatures; [a]asymmetric; [s]symmetric; and [d]deformation (Paper 5)

Raman-active modes	Intensity	Raman shift / cm^{-1} This work	Raman shift / cm^{-1} Other works (theory)	Ref.
Combination and overtones	medium	1386.2	1359/1363	[71, 83]
$B_{2g}(\nu_a)$ (CrO_2)	medium	680.9	660	[87]
$E_g(\nu_d)$	medium/weak	610.8	602 (615)	[82, 83]
$A_{1g}(\nu_s)$	very strong	551.4	544 (554)	[82, 83]
$E_g(\nu_d)$	weak	543	518 (528)	[82, 83]
$E_g(\nu_d)$	medium	349.4	348 (350)	[82, 83]
$E_g(\nu_d)$	medium	307.5	304 (296)	[82, 83]
$A_{1g}(\nu_s)$	N/A	Not observed	(266)	[82]*
$E_g(\nu_d)$	N/A	Not observed	(235)	[82]*

Effects of Raman laser power

The conversion of $Cr(OH)_3$ and Cr_2O_3 films into the crystalline oxide phase with increasing laser power (Figure 14) was also investigated. Nanoparticles were irradiated at several laser powers, increasing from 0.035 to 7.0 mW (Figure 16). As the laser power increased, the Raman spectra of $Cr(OH)_3$ nanoparticles changed from the amorphous hydroxide phase to the crystalline α-Cr_2O_3 phase (Figure 16a); a result very similar to that of the deposited $Cr(OH)_3$ film (Figure 14a). Opposed to that, the spectra of Cr_2O_3 nanoparticles excited with different laser powers (Figure 16b) did not reveal the same transition as those observed for the film. Peaks related to the oxide phase were already observed at 0.035 mW, and no correlation with the electrodeposited Cr_2O_3 (Figure 14b) was found.

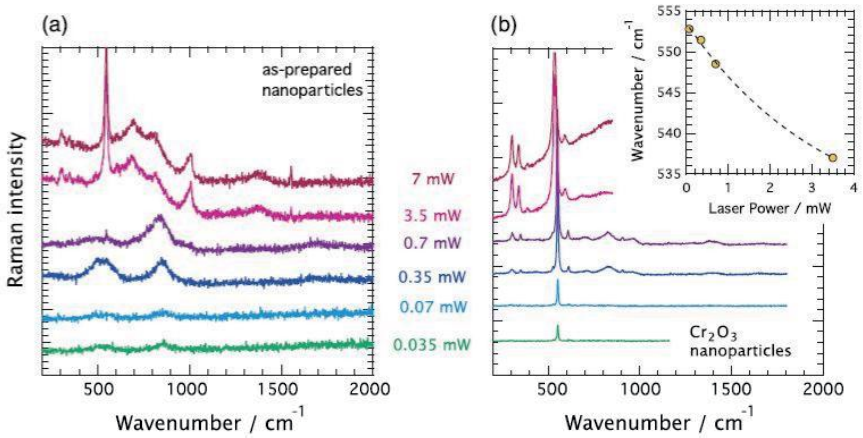

Figure 16 – Raman spectra with increasing laser power collected from a) $Cr(OH)_3$ nanoparticles and b) Cr_2O_3 nanoparticles. Inset: Effect of laser power on the peak position of the Raman signature at ~551 cm^{-1} (taken at 0.7 mW) (Paper 5).

The phase transition that occurred upon increasing laser energy, and was observed in Figures 14a, 14b and 16a, was rationalized to be due to a local heating effect caused by light absorption. This hypothesis was proposed as this effect has already been reported using more powerful lasers [87-93]. Only Fazio et al. [94] has reported the transformation of oxides using low laser powers**.** To verify that a heating effect from light absorption also occurred in the case of $Cr(OH)_3/Cr_2O_3$, Raman spectra of the $Cr(OH)_3$ nanoparticles (Figure 17a) and Cr_2O_3 nanoparticles (Figure 17b) were recorded at increasing temperatures. The laser energy used in this case was 0.35 mW, as at this power no phase transition has occurred (Figure 16a). The transition from $Cr(OH)_3$ to the oxide begins at 200 ºC, where the peak at 530 cm^{-1} start to disappear. At 300 ºC, nothing remains of the characteristic peaks of the $Cr(OH)_3$, and a tiny peak for the oxide is observed. However, the transformation is not complete at 390 ºC, and the full spectrum for the crystalline Cr_2O_3 is observed only at 425 ºC. The results in Figure 17a align with those in Figure 16a, where the Raman spectra also exhibit stepwise changes before a complete phase transition occurred.

The Raman spectra collected from Cr_2O_3 nanoparticles do not dramatically change upon heating of the samples (Figure 17b). However, the high-intensity peak changes systematically with increasing temperature. This shift is also shown in Figure 16b and is clearly shown in the figure

inset. The Raman peak positions in the inset of Figure 16b are also presented in the inset of Figure 17b (as yellow dots), where the peak positions as a function of temperature (green dots) are plotted. Laser power and temperature are clearly correlated. At 0.7 mW of laser power (dotted yellow line), the peak was positioned at 551.2 cm^{-1}, which corresponds to a temperature of 150 °C. At 3.5 mW, the peak is positioned at 537 cm^{-1} (Figure 16b, inset), which is beyond the shift caused by temperature up to 450 °C. Hence, it can be expected that a laser power of 3.5 mW causes a temperature increase higher than 450 °C. Further investigations of the thermodecomposition of $Cr(OH)_3$ were performed with TGA/DSC measurements (Paper 5). Dehydration of $Cr(OH)_3$ occurred in four steps, in accordance with the literature [72, 95-100]. The TGA/DSC analysis showed that a CrOOH phase is probably formed prior to full crystallization to Cr_2O_3 at 409 °C. A laser power of 3.5 mW can thus generate enough heat to promote the conversion of the amorphous $Cr(OH)_3$ to crystalline Cr_2O_3, validating the proposed local heating effect caused by laser absorption.

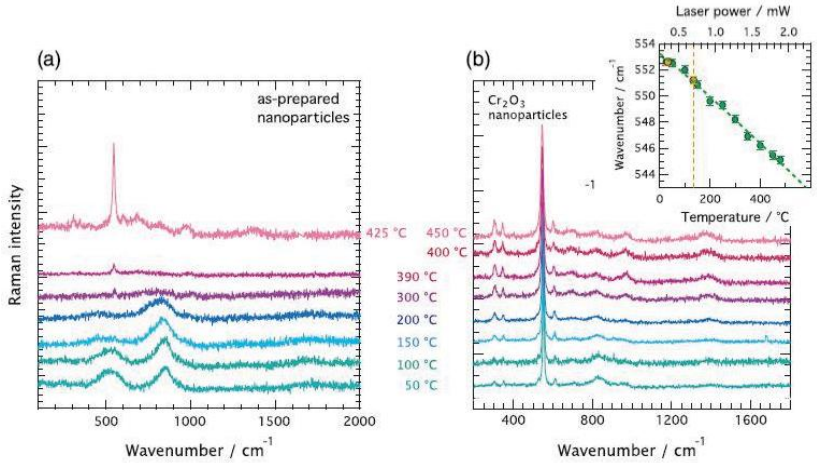

Figure 17 – Raman spectra of $Cr(OH)_3$ nanoparticles (a) and Cr_2O_3 nanoparticles (b) as a function of increasing temperature. Inset: Effect of temperature (bottom axis) and laser power (top axis) on the peak position of the 551 cm^{-1} Raman signature. All spectra were collected at 0.35 mW (Paper 5).

4.3. Summary

The identification of ex situ-formed $Cr(OH)_3$ and Cr_2O_3 films was carried out using SEM, EDX and Raman spectroscopy. SEM images were very similar to those previously obtained [62, 66]; the authors of those studies identified pure phases using XPS. Combining SEM, EDX, and Raman results creates a strong case to confirm the successful generation of separate phases of $Cr(OH)_3$ and Cr_2O_3. The electrochemical reactions relevant to the chlorate process were consequently analysed and interpreted according to the surface structure, morphology and active area of these materials, as it will be seen in the following sections.

5. Electrochemical results

The ex situ electrodeposition of various Cr(III) oxides opened the possibility to investigate electrochemical reactions on well-characterized electrodes. Not only the blocking mechanism but also the mechanism for allowing the HER must be understood to explain the selectivity provided by chromium film. Four of the papers covered by this thesis studied hypochlorite reduction and the HER on electrodes covered with either $Cr(OH)_3$ or Cr_2O_3. The inhibition mechanisms in which hypochlorite reduction is avoided were investigated in Paper 1, while Paper 2 focused on the kinetics of the HER. In Paper 3, the HER kinetics were investigated as a function of different degrees of Cr substitution into a $Fe_{1-x}Cr_xOOH$ structure. Paper 4 returned to a discussion of the hypochlorite reduction, and the blocking mechanism was revised and determined. The results presented in these four papers bring new valuable information that will help all chlorate producers in the search for a suitable replacement for sodium dichromate.

5.1. The hydrogen evolution reaction

The HER is the desired reaction in the chlorate process. This reaction is also called water reduction because it occurs under alkaline conditions. In this section, the kinetics and mechanisms of water reduction on $Cr(OH)_3$ and Cr_2O_3 will be carefully evaluated.

5.1.1. HER on $Cr(OH)_3$ and Cr_2O_3 deposited on Ti electrodes

The HER was investigated by LSV (Figure 18) and steady-state polarization techniques (Figure 19) using a Ti RDE and Ti electrodes covered with $Cr(OH)_3$ ($Cr(OH)_3$@Ti) or Cr_2O_3 (Cr_2O_3@Ti). The $Cr(OH)_3$@Ti electrode displayed a higher overpotential than Cr_2O_3@Ti and Ti for the HER. Differences in kinetics were more clearly shown when the results in Figure 19 were fitted with Equation 21 and kinetic parameters were obtained (Table 5). The rate constant (k) was three orders of magnitude larger for the oxide than for the hydroxide.

The differences in kinetics can be explained in the context of surface areas and reaction mechanisms. The surface area was larger for the Cr_2O_3@Ti film than $Cr(OH)_3$@Ti, as indicated by SEM images (Figure 13). This observation was confirmed by measurements (Paper 2) that

showed that the capacitance of the Cr_2O_3 layer was three orders of magnitude larger than that of the $Cr(OH)_3$ film.

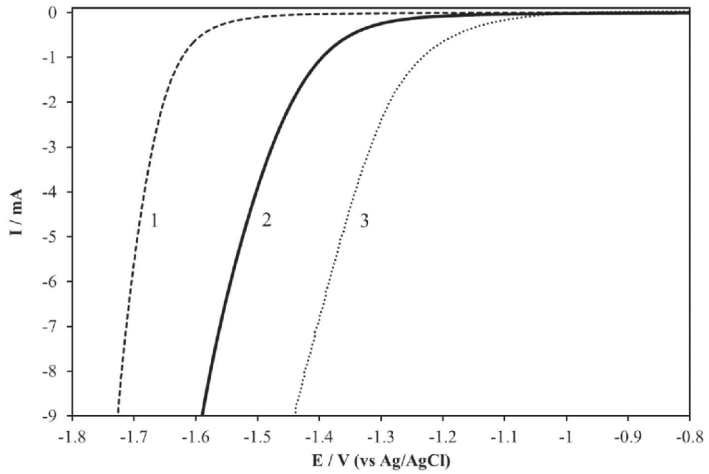

Figure 18 – Water reduction currents measured for: $Cr(OH)_3$@Ti (1), Ti (2) and Cr_2O_3@Ti (3) electrodes in 0.2 M $NaSO_4$ supporting electrolyte at pH 11. Sweep rate of 5 mV s^{-1} and electrode rotation rate of 3000 rpm (Paper 2).

Another explanation for the different kinetics lies in the reaction mechanism. The general HER mechanism on oxides is given in Equations 30a-d [101]. Equation 30a depicts the acid-base equilibrium every oxide undergoes in aqueous solution, while Equations 30b-d denote the Volmer-Heyrovsky-Tafel mechanism on an oxide electrode. The high Tafel slopes in Table 5 indicate that a first electron transfer limits the reaction rate for both $Cr(OH)_3$ and Cr_2O_3, meaning that Equation 30b is the rate-determining step (r.d.s.). However, the low α value for the Cr_2O_3 electrode suggests that the structure of the activated complex is closer to that of the products than that of the reactants. This product-like structure is explained by the lack of water in the Cr_2O_3 structure and the involvement of only surface water in the reaction is expected. In contrast, α values were closer to 0.5 for the $Cr(OH)_3$ surfaces, and the related transition state lies between H_2O and H_2.The structure of the activated complex suggests that structural water is involved in the reaction and must be replaced to maintain an intact film structure. This exchange of water is

slow due to the slow ligand exchange reaction of $Cr(OH)_3$ [102] and thus explains the low rate constant for water reduction on the hydroxide phase.

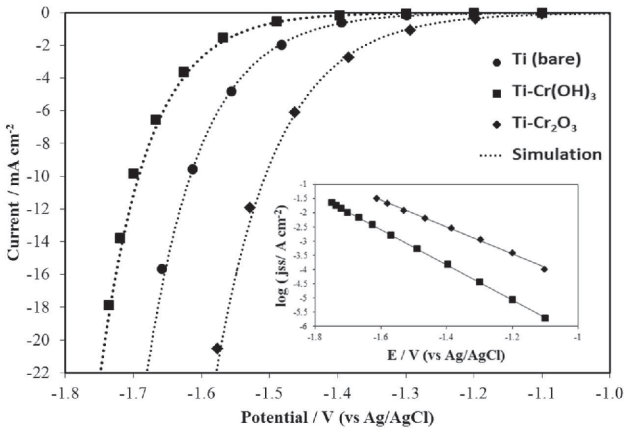

Figure 19 – Steady-state polarization measurements (symbols) fitted with Equation 21 (dotted line). Inset: Tafel plots. In 0.2 M $NaSO_4$ electrolyte at pH 11. Electrode rotation rate: 3000 rpm (Paper 2).

Table 5 – Kinetic parameters for water reduction on Ti electrodes uncovered or covered with Cr_2O_3 or $Cr(OH)_3$ (Paper 2).

	Tafel slope§ mV dec^{-1}	**Charge-transfer coef. (α)§**	**Reaction rate (k)* mole cm^{-2} s^{-1}**
Cr_2O_3	239(±27)	0.25(±0.03)	$2.3(\pm1.5)\text{x}10^{-10}$
$Cr(OH)_3$	145(±28)	0.41(±0.06)	$9.9(\pm12)\text{x}10^{-13}$
Ti	180	0.31	$8.0\text{x}10^{-12}$

§ Experimentally obtained * Simulated values

$$\equiv Cr-OH_2^+ + H_2O \leftrightarrow \equiv Cr-OH + H_3O^+ \quad K_{a1}$$
$$\equiv Cr-OH + H_2O \leftrightarrow \equiv Cr-O^- + H_3O^+ \quad K_{a2} \qquad (30a)$$

$$\equiv Cr-OH_2^+ + e^- \leftrightarrow \equiv Cr-OH_2 \qquad (30b)$$

$$\equiv Cr-OH_2 + H_2O + e^- \rightarrow \equiv Cr-OH + H_2 + OH^- \qquad (30c)$$

$$2 \equiv Cr-OH_2 \leftrightarrow \equiv Cr-OH + H_2 \qquad (30d)$$

Findings presented in Figures 18 and 19 can be placed in the context of chlorate production when compared to previous results from in situ-formed films. The increase in the HER overpotential caused by $Cr(OH)_3$, can be compared to that observed with in situ-formed films as presented in [9, 11, 12]. Accordingly, this result offers another proof that the in situ chromate reduction yields a $Cr(OH)_3 \times xH_2O$ film. Moreover, Cornell et al. [9] proposed a dual composition for the film where an inert outer layer of $Cr(OH)_3$ and an active inner layer of Cr_2O_3 were formed. This concept agrees with the findings in presented here, in the sense that the activity towards the HER is much higher on the oxide than on the hydroxide phase.

5.1.2. Influence of the substrate on the HER at $Cr(OH)_3$

In Paper 4, the HER was investigated on $Cr(OH)_3$@Au, $Cr(OH)_3$@Fe and $Cr(OH)_3$@Ti, and their respective polished electrodes using LSV (Figure 20). The potential scans were taken from the negative to the positive direction at 2 mV s^{-1} in 0.2 M Na_2SO_4 solution containing 1 mM NaOH. Figure 20a shows water reduction at the pure metal surfaces, and Figure 20b shows water reduction at electrodes covered with $Cr(OH)_3$. The activity for water reduction on pure metals decreased in the order: Fe > Au > Ti (Figure 20a). On electrodes covered with $Cr(OH)_3$, the order was changed; $Cr(OH)_3$@Au was the most active surface, and $Cr(OH)_3$@Ti was the least active. The activity order thus became $Cr(OH)_3$@Au > $Cr(OH)_3$@Fe > $Cr(OH)_3$@Ti (Figure 20b).

The $Cr(OH)_3$@Au electrode is more active than the pure Au metal, which was the same relation observed with films formed in situ on Au [12]. This fact cannot be ignored and clearly demonstrates that the reaction occurs on the film and not on the substrate. Oppositely to the case of Au electrodes, the overpotential for the HER on Fe and Ti electrodes was higher for covered than uncovered surfaces, which was also in agreement with results from Cr films formed in situ on Pt [12] and Fe [9] electrodes. These results indicate that the ex situ-electrodeposited $Cr(OH)_3$ strongly reproduced the features of in situ-formed films.

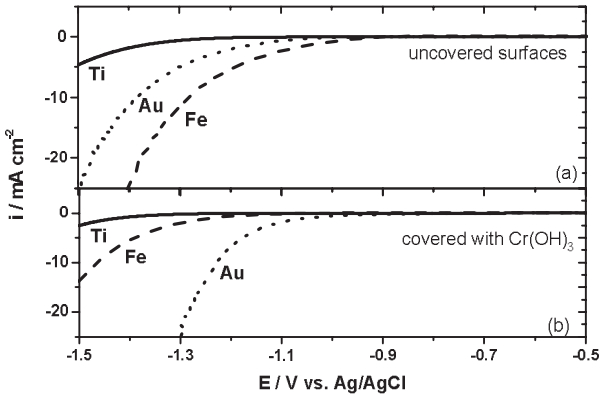

Figure 20 – Hydrogen evolution reaction investigated on Au (dotted line), Fe (dashed line) and Ti (solid line) electrode bare surfaces (a) or surfaces covered with $Cr(OH)_3$ (b). The electrolyte was 0.2 M Na_2SO_4 at pH = 11. The electrode rotation rate was 2000 rpm, and the sweep rate was 2 mV s^{-1} (Paper 4).

5.1.3. Hydrogen evolution on mixed $Fe_{1-x}Cr_xOOH$

To increase understanding and to bridge the findings of ex situ-formed films to the real chlorate process, the impact of Cr substitution in FeOOH on the HER kinetics was investigated. In real chlorate cells, the HER occurs on heavily corroded mild steel electrodes. The main corrosion products have been identified to be α-FeOOH and γ-FeOOH [33]. During electrolysis, these compounds are reduced to $Fe(OH)_2$, and when the current is switched off, Fe(II) is once again oxidized to Fe(III) [101]. A pilot plant study has revealed that in this oxidation-reduction cycle, considerable amounts of Cr are incorporated in the iron oxide structure [42] since Fe(II) is a potent scavenger for Cr(VI) [103]. The kinetics of the HER on goethite (α-FeOOH) whose Fe had been isomorphically substituted with Cr were thus investigated in Paper 3. The α-$Fe_{1-x}Cr_xOOH$ compounds were prepared by the method proposed by Schwertmann et al. [104]. This method allowed the synthesis of mixed Fe-Cr oxyhydroxides with different degrees of substitution. Sample characterizations are given in Paper 3.

The atomic composition of the samples (in %) was analysed by x-ray fluorescence (XRF), yielding Cr content of 0 (Sample 1), 0.54 (Sample 2), 1.15 (Sample 3), 1.61 (Sample 4) and

2.75 at% (Sample 5). Electrochemical measurements were carried out by means of steady-state polarization techniques (Figure 21a) and LSV (Figure 21b). The steady-state sweeps in Figure 21a show a clear trend of increasing HER overpotential with increasing Cr content. Figure 21b shows LSV of bare Fe, Sample 1, and an Fe/$Cr(OH)_3$ (denoting an Fe electrode covered with $Cr(OH)_3$) and reveals that bare Fe displayed the lowest HER overpotential and Fe/$Cr(OH)_3$ the highest. The overpotential for Samples 1 and 5 appeared between that of pure Fe and Fe/$Cr(OH)_3$.

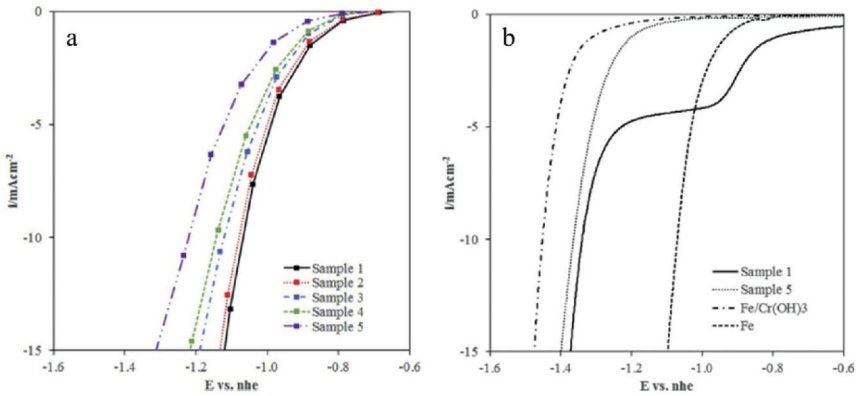

Figure 21 – a) Water reduction currents obtained during steady-state polarization on electrodes prepared with Samples 1-5. Sample 1 = FeOOH, Sample 2 = 0.54 at% Cr, Sample 3 = 1.15% Cr, Sample 4 = 1.61 at% Cr and Sample 5 = 2.75 at% Cr. b) Linear sweep voltammetry on $Fe_{1-x}Cr_xOOH$, Fe and Fe covered by $Cr(OH)_3$ (Paper 3).

The increase in overpotential with increasing Cr content in α-$Fe_{1-x}Cr_xOOH$ (Figure 21a) shows that Cr has a deleterious effect on the HER. This effect has two reasonable explanations. The first effect is related to the slowed kinetics towards the HER displayed by $Cr(OH)_3$. With increasing Cr-content, more Cr terminated sites are expected to be present. These sites are less active than Fe-terminated sites, therefore increasing the overpotential.

The second effect is related to stabilization of the Fe(III) in the α-$Fe_{1-x}Cr_xOOH$ structure. Hedenstedt et al. [101] demonstrated that the active phase for the HER in FeOOH is the reduced form, $Fe(OH)_2$. This is also evidenced in Figure 21b, Sample 1, where a reduction wave is observed prior to the HER. In the presence of 2.75 at% Cr in the FeOOH structure (Figure 21b, Sample 5), the reduction of Fe(III) to Fe(II) is suppressed as the reduction wave vanishes. Thus,

the number of active sites (composed of Fe(II)) is dramatically decreased and, hence, the HER overpotential increases. As an immediate conclusion, corroded Fe in real electrolysers will also be to some extent deactivated by Cr(III), because Cr stabilizes Fe(III) in the oxyhydroxide structure.

5.2. Summary of the effects on the HER

The results from $Cr(OH)_3$ and Cr_2O_3 films deposited ex situ on Ti clearly indicate that Cr_2O_3 displays higher catalytic activity than $Cr(OH)_3$ towards the HER. Moreover, the study of $Cr(OH)_3$ deposited on different metals has shown that the film controls the catalytic properties of the electrodes. This result clearly demonstrates that the HER occurs on the film and not on the underlying substrate. The fact that $Cr(OH)_3$ and Cr_2O_3 are active towards water reduction agrees well with findings on in situ-formed films. However, what makes Cr(III) films unique is their ability to block unwanted reactions, as will be now discussed.

5.3. Hypochlorite reduction: experiments and theory

Inhibition of hypochlorite reduction is necessary to achieve a high current efficiency in the chlorate process. This inhibition is unquestionably achieved by in situ-formed Cr(III) films (Section 2.5.6), but its mechanism is still not well understood. Hypochlorite reduction on well-characterized ex situ-formed $Cr(OH)_3$ and Cr_2O_3 films was thus studied in detail in this thesis.

Investigations of hypochlorite reduction were performed by means of LSV in 0.2 M Na_2SO_4 supporting electrolyte at pH 11 with 70 mM of hypochlorite. In Paper 1, studies were carried out using Ti electrodes, and on pure phases of $Cr(OH)_3$ or Cr_2O_3 that were electrodeposited onto Ti. In Paper 4, the study was extended to investigate hypochlorite reduction on $Cr(OH)_3$ films placed on different substrates.

LSV measurements using Ti and Ti covered with $Cr(OH)_3$ or Cr_2O_3 in solution containing hypochlorite are shown in Figure 22. In the absence of the Cr(III) films, hypochlorite reduction readily occurs on bare Ti (solid line), in contrast to the cases where Ti is covered with either $Cr(OH)_3$ (dashed line) or Cr_2O_3 (dotted line). The presence of the films completely inhibits hypochlorite reduction, and the inhibition is independent of the structure of the films.

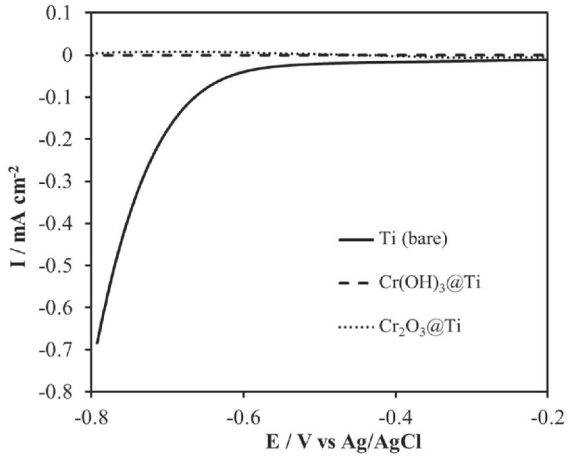

Figure 22 – Potential sweeps in the negative direction of Ti electrodes with and without electrodeposited Cr(III) layers in the presence of 70 mM hypochlorite in 0.2 M Na_2SO_4, pH 11. The sweep rate was 5 mV s^{-1}, and the rotation rate was 3000 rpm.

The interpretation of the blocking provided by $Cr(OH)_3$ and Cr_2O_3 on Ti electrodes can be challenging by the fact that Ti is not a good electrocatalyst for hypochlorite reduction. Additionally, its technical relevance can be questioned because few current chlorate production technologies use Ti cathodes [27, 105]. Therefore, the reduction of hypochlorite was investigated on other electrode materials, such as Fe and Au both uncovered and covered with $Cr(OH)_3$ films, to obtain additional information about the blocking effect (Paper 4).

The morphology and composition of electrodeposited $Cr(OH)_3$@Me (Me = Au, Fe or Ti) were determined by SEM images (Figure 23), and surface compositional analyses were performed with EDX (Table 6). The morphology of the electrodeposited films on Au (Figure 23a) differs from those obtained for films on Fe (Figure 23b) and Ti (Figure 23c), which are somewhat similar.

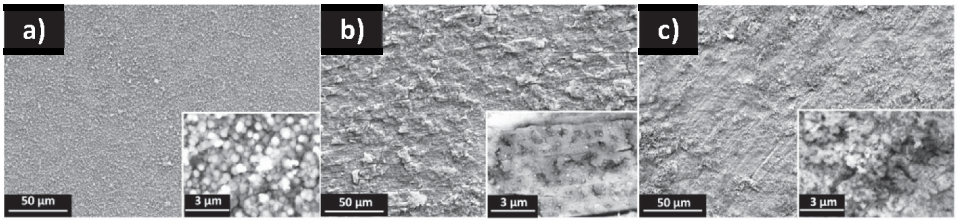

Figure 23 – SEM images of $Cr(OH)_3$ electrodeposited on a) Au, b) Fe and c) Ti (Paper 4). Inset: SEM images at higher magnifications (Paper 4).

EDX shows that high amounts of Cr are present in $Cr(OH)_3$@Au at nearly a 1:1 ratio to O. In contrast, $Cr(OH)_3$@Fe presents a 1:2.3 ratio, which is the closest of the three sample values to the desired 1:3. These results indicate that the films formed on Au and Fe are not composed of pure $Cr(OH)_3$ and that Cr with valences lower than +3 might be present. The Cr:O ratio in the film on Ti shows a high O content. A thicker TiO_2 film might have formed during the electrodeposition of $Cr(OH)_3$ on Ti.

Table 6 – Surface compositional analyses of $Cr(OH)_3$ electrodeposited on Au, Fe and Ti (Paper 4).

	Substrate / at%	Cr / at%	O / at%	Impurities / at%	Ratio Cr:O
$Cr(OH)_3$@Au	<1	53	40	6*	1:0.75
$Cr(OH)_3$@Fe	~9	26	59	6*	1:2.3
$Cr(OH)_3$@Ti	~25	5	64	6*	1:12

Figure 24 shows the results of studying the reduction of hypochlorite at different electrodes using LSV. Voltammograms recorded using electrodes without $Cr(OH)_3$ (Figure 24a) show that all three surfaces are capable of reducing hypochlorite, with Au as the most active surface. The scenario changes completely when the electrodes are covered with $Cr(OH)_3$ (Figure 24b). The reduction of hypochlorite is completely blocked in all cases. This result indicates that ex situ formed-$Cr(OH)_3$ supresses this reaction at highly active electrodes. Moreover, the blocking effect is independent of the morphology and composition of the films.

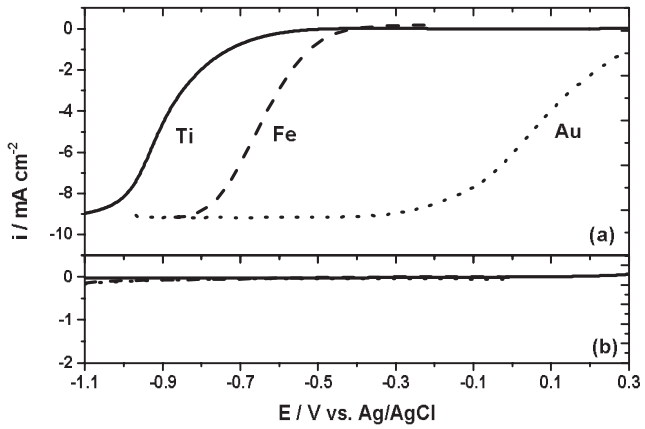

Figure 24 – Hypochlorite reduction on Au (dotted), Fe (dashed) and Ti (solid) in 0.2 M Na_2SO_4, pH 11. The sweep rate was 5 mV s^{-1}, and the rotation rate was 2000 rpm. Hypochlorite was added to a concentration of 5 mM. a) polished surfaces; b) electrodes covered with $Cr(OH)_3$ (Paper 4).

Cr(III) films were shown here to be efficient in blocking hypochlorite reduction independent of their composition, morphology, thickness and molecular structure. This effect is thus intrinsically connected to the chemical and/or electrochemical characteristics shared by $Cr(OH)_3$ and Cr_2O_3. In the literature, the inhibition of hypochlorite reduction has been discussed in the context of a physical barrier [9, 11, 12, 19] or an adverse potential gradient [16]. Here, these theories are revisited and elaborated in terms of electrocatalysis, semiconductor properties and surface charges. Mechanistic insights regarding the electrocatalytic aspects of hypochlorite reduction are based on DFT calculations (Papers 1 and 4). In the following sections, a more thorough explanation will be given, and an understanding of the blocking mechanism is obtained when Cr oxides are compared with Fe oxides.

5.3.1. Surface charge

In Paper 1, hypochlorite reduction was investigated on Ti electrodes covered with α-FeOOH, γ-FeOOH, Cr_2O_3 or $Cr(OH)_3$. Hypochlorite reduction proceeded with a rather high rate on the Fe-based electrodes but was completely supressed by the Cr(III) films. Discussions on the blocking

mechanism started by comparing the surface charge of Cr(III) oxides with that of Fe(III) oxyhydroxides.

The surface charge of oxides in solution is determined by the solution pH. Metal oxides undergo an acid-base reaction in aqueous solutions (Equation 30a, Section 5.1.1). The pK_a for this reaction is equal to the pH value where the net charge of the oxide is zero, i.e., the point of zero charge (PZC). The PZC is specific for each metal oxide and can be calculated [106] or experimentally obtained [107-110]. The PZCs of α-FeOOH, γ-FeOOH, Cr_2O_3 and $Cr(OH)_3$, compiled in Table 7, indicate that all surfaces investigated in Paper 1 are negatively charged at the pH 11 (the pH used in this study). Similarly, these compounds are expected to present negatively charged surfaces in the real chlorate process due to the high pH in the vicinity of the cathodes (Section 2.1).

Table 7 – Point of zero charge for the studied Fe(III)-oxyhydroxides [108] and Cr(III) oxide and hydroxide [110] (Paper 1).

Species	α-FeOOH	γ-FeOOH	Cr_2O_3	$Cr(OH)_3$
PZC	8.6 ± 0.8	7.1 ± 0.7	7.0 ± 1.6	7.9 ± 1.2

The pK_a for the $HClO/ClO^-$ couple is 7.53, which means the anion dominates at alkaline pH values. In this case, the reduction of the hypochlorite on negatively charged surfaces is thus partly hampered by electrostatic repulsion and the adverse potential gradient. However, these effects have been shown to be insufficient to stop hypochlorite reduction on Fe oxides. They should thus also not play a large role in the case of Cr(III)-covered electrodes. Accordingly, this results are in agreement with the conclusions of Kolthoff and Shams El Din [19] and Lindbergh and Simonsson [12], and the effect of the adverse potential gradient can once again be ruled out as the only explanation for the blocking mechanism.

5.3.2. Semiconducting properties

Effects from the electric properties of the film have never been considered in this context. In Paper 1, the semiconducting properties of Cr(III) and Fe(III) were compared. Cr(III) oxides commonly present p-type behaviour [111-113] due to metal deficiencies in the structure, but they

can also assume n-type behaviour in special cases [113, 114]. On the other hand, Fe oxyhydroxides and oxides are well known to behave as n-type semiconductors. n-Type semiconductors are electron donors, supporting reduction reactions. Thus, hypochlorite reduction on Fe oxyhydroxide electrodes should be unproblematic, as proved in Paper 1. However, p-type semiconductors are hole carriers, meaning that the conduction band is empty of electrons and that they are more likely to support oxidation reactions. Hypochlorite reduction is, therefore, expected to be hampered by p-type semiconductors such as $Cr(OH)_3$ and Cr_2O_3 films. This fact also explains why the reduction of other chemicals compounds, including O_2 [12, 41], Fe^{3+} [12, 19] and others [19], are also blocked.

Interestingly, the HER proceeds on the Cr(III) films (Section 5.1), indicating that the semiconducting properties do not explain the entire blocking mechanism, especially not at high potentials.

5.3.3. Determination of the blocking mechanism by DFT calculations

As surface charge and semiconducting properties do not fully explain the mechanisms blocking hypochlorite reduction by Cr(III) oxide films, DFT calculations were used to develop new insights. In Paper 1, the focus was placed on the mechanism of O – Cl bond breaking, assuming that the recovery of the catalyst occurs through the reduction of the oxidized active site. In Paper 4, elementary steps for splitting O – Cl were neglected, and the recovery of the catalyst was more thoroughly investigated.

Calculations were performed on model surfaces where either Cr or Fe replaced Mg in a $MgO_y(OH)_x$ test rig (Paper 1). The r.d.s. for hypochlorite reduction was determined from Tafel slopes of FeOOH activity (Paper 1). A value close to -120 mV dec^{-1} was observed, which indicates that the first electron transfer is the r.d.s. This first electron transfer in hypochlorite reduction results in adsorption of Cl on the metal oxide surface, which will be discussed below.

The mechanism proposed for hypochlorite reduction in Paper 1 is presented in Figure 25. In Figure 25a, every step of the reaction mechanism is depicted (a, b, c, d and e), while the energy required for each step is given in Figure 25b. The first step is the adsorption of hypochlorite onto a *-OH site at the surface through Cr – O bond formation (step a). The first electron transfer

causes the O – Cl bond to split since all bonding and anti-bonding molecular orbitals in the OCl^- molecule are then filled with electrons. As a result from the binuclear mechanism assumed, chloride adsorbs on an adjacent site at the surface (step b). The subsequent steps depicted in Figure 25a are related to the recovery of the hydroxide surface.

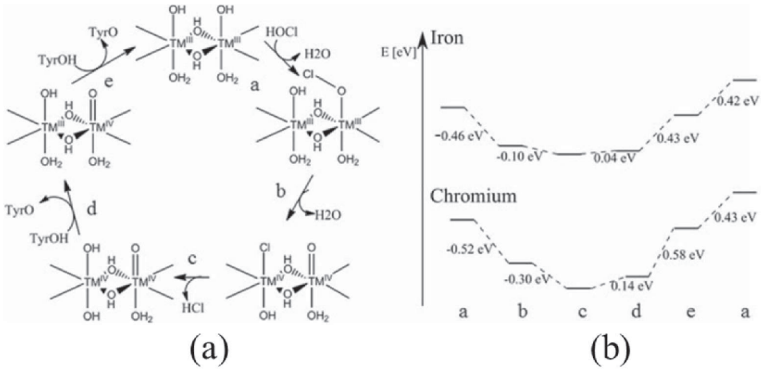

Figure 25 – Reduction cycle for hypochlorite reduction on Fe and Cr oxides (Paper 1).

In Paper 1, the energy related to the adsorption of Cl^- was considered to be critical to determine whether hypochlorite reduction proceeds on Fe(III) oxides and Cr(III) oxides. The energy of each step, presented in Figure 25b, shows that the energy profile for both Cr(III) and Fe(III) are similar, and no differences regarding OCl^- reduction should be expected. As also shown in Paper 1, the energy of adsorption of chloride on Cr(III) and Fe(III) differs of only 0.03 eV, and it is too small to account for the large differences observed experimentally (Paper 1). These results mean that both, Fe(III) and Cr(III), sites should perform equally regarding the hypochlorite reduction and both should be active.

As no thermodynamic difference between Fe(III) and Cr(III) were found in the splitting of the O – Cl bond, yet strong experimental evidences that Cr(III) display a blocking effect, the reaction mechanism from Figure 25 was re-evaluated (Paper 4). In the new proposed, simplified mechanism (Figure 26), the elementary steps for bond breaking were neglected, and the focus was in the surface regeneration. The reduction of hypochlorite begins, as before, with the adsorption of hypochlorite to a TM active site, causing oxidation of the metal. After this step, the O – Cl bond will be split, causing a further oxidation of the surface, forming a TM = O site.

(Here, the fate of the Cl^- was disregarded). The unstable TM = O must be further reduced, and it occurs via two consecutive reduction reactions for the recovery of the TM active site (Figure 26).

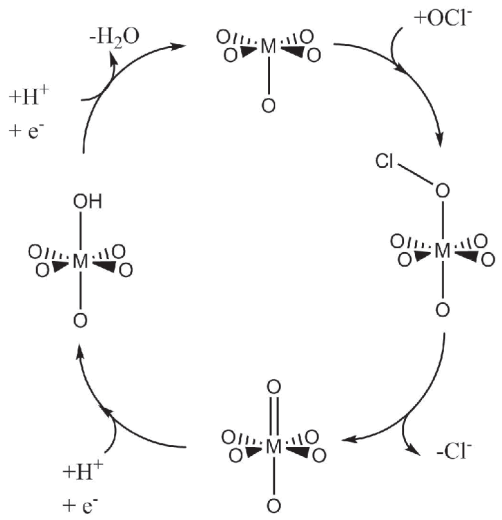

Figure 26 – The mechanism for ClO^- reduction on metal oxides (Paper 4).

Through the mechanism presented in Figure 26 and DFT calculations, a new energy diagrams for hypochlorite reduction on Cr oxides and Fe oxides was built (Figure 27). This new system considers a $Fe(OH)_2$ slab as the active site for water reduction, since it is the most probable structure in the real process [101]. $Cr@Fe(OH)_2$ and $Fe@Fe(OH)_2$ denote Cr- or Fe-terminated sites, respectively. Figure 27 shows that the adsorption of chloride, cleavage of the O – Cl bond and reduction of Me = O to TM – OH are unproblematic from the energetic point of view for both surfaces. However, the scenario changes in the last reaction step when the TM – OH has to be further reduced. The reduction of Fe – OH sites requires 0.37 V, which is feasible in the potential range where water reduction occurs. On the other hand, a potential of -1.3 V is required to reduce Cr – OH sites, and this is considered too high to be achieved at water reduction potentials. In addition, the poor conductivity of $Cr(OH)_3$ will shift the potential to even more negative potentials. Therefore, the reduction of hypochlorite at Cr(III) films is blocked by OH irreversibly adsorbed on the surface.

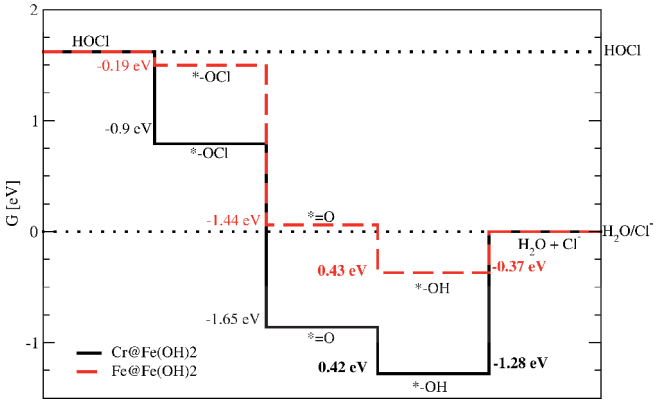

Figure 27 – Energy diagram for hypochlorite reduction on $Fe@Fe(OH)_2$ and $Cr@Fe(OH)_2$. Electrochemical steps are indicated in bold (Paper 4).

5.4. Summary of hypochlorite reduction

Hypochlorite reduction was completely avoided in the presence of $Cr(OH)_3$ or Cr_2O_3 films. Even good electrocatalysts for hypochlorite reduction such as Au and Fe became inactive when covered with a $Cr(OH)_3$ film. A blocking mechanism based on acid-base and semiconducting properties has been shown to be limited and cannot fully explain a total lack of hypochlorite reduction on Cr(III) oxides. DFT calculations have shown that both Cr(III) and Fe(III) are active in reducing hypochlorite once chlorides adsorb on the active site. A blocking mechanism was thus rationalized to be related to the recovery of the catalyst, which is unfeasible for Cr(III) at water reduction potentials.

5.5. The selectivity mechanism

Ex situ-electrodeposited Cr(III) oxide/hydroxide films demonstrated the same striking ability as in situ-formed films to block hypochlorite reduction. This effect was caused by blockage of the active site by OH. However, these blocked sites for hypochlorite reduction can still act as active sites for hydrogen evolution, indicating that a selective mechanism can be proposed. Based on the mechanisms proposed by Hedenstedt et al. [101] and Trasatti [115-117], water reduction on oxides occurs at TM – OH sites (see Equation 30b-d). Combining the mechanism of water reduction on metal oxides with the blocking mechanism proposed in Figure 26, a mechanism

leading to the selectivity towards water reduction can be proposde (Figure 28). In the waterborne system of the chlorate process, the Cr – OH surface will be dominant (see Figure 6, Paper 3), and the water reduction cycle (highlighted in red) proceeds.

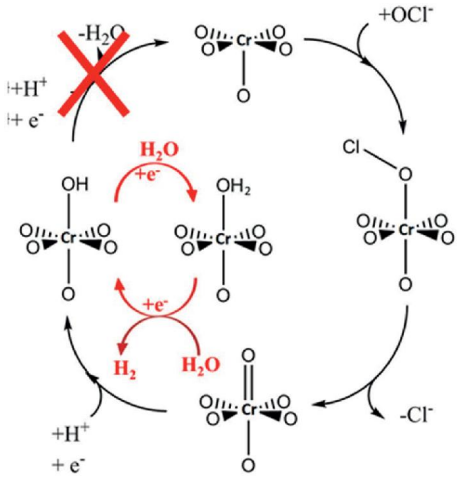

Figure 28 – The selective mechanism provided by $Cr(OH)_3$ towards the hydrogen evolution reaction.

6. A link between two worlds

The $Cr(OH)_3$ and Cr_2O_3 ex situ-formed films, investigated in this thesis, displayed the same behaviour as those expressed by in situ-formed Cr(III) films. Results led to proposing a mechanism in which selectivity on chlorate cathodes is provided (Figure 28). The knowledge, however, is not limited to benchtop experiments, and this chapter aims to explain how it applies to the real process.

The most relevant result in this thesis concerns the explanation of the mechanism for selective water reduction at the cathode. The mechanism implies that covering the whole cathode with a monolayer of Cr(III) oxide is sufficient to completely block hypochlorite reduction. It explains why high selectivity has been seen experimentally even using very small concentrations of dichromate, ranging from few grams for Fe [15, 42] to µM concentrations for polished Ti and steel electrodes [50].

At chlorate plants, however, concentration of 2 to 7 g dm^{-3} of sodium dichromate is commonly present in the electrolyte (Table 1) to ensure high production yields. Obviously, in real electrolysers, water reduction takes place at severely corroded cathodes, which have a huge active surface area. Therefore, covering all cathode blades demands a higher amount of chromium compared to that of polished surfaces. Still, the total amount of chromium in the process exceeds that needed to cover the cathodes.

The surplus of Cr can be explained by other technical demands. A high amount of Cr(VI) is needed to minimize mass-transfer limitations and ensure fast film formation. Additionally, the film is not stable during electrolysis; instead, it is probably continuously destroyed by the vigorous hydrogen evolution and the extremely oxidizing environment. Consequently, it must be in situ renewed. Finally, Cr(VI) has other beneficial effects on the chlorate process, as summarized in Section 2.5, and these reasons explain why the currently used concentration of dichromate is significantly larger than the estimated requirement needed to fully provide selectivity.

7. Conclusions

In this work, the selectivity provided by sodium dichromate in the chlorate process was investigated on well-characterized ex situ-formed $Cr(OH)_3$ and Cr_2O_3 films. The hypochlorite reduction was found to be completely blocked irrespective of the composition or morphology of the films. Still, the films actively reduce water, and the rate for this reaction depends on the molecular structure and morphology of the deposited films. This conclusion was evidenced by Cr_2O_3 having higher HER catalytic activity than $Cr(OH)_3$.

Cr has deleterious effects on the HER on $Fe_{1-x}Cr_xOOH$ compounds. Compounds with higher Cr content require larger overpotentials to drive the water reduction reaction. This behaviour was explained by the slow HER kinetics on $Cr(OH)_3$, combined with the stabilization of Fe(III) in the $Fe_{1-x}Cr_xOOH$ structure, avoiding formation of the Fe(II) active site for the HER.

The fact that the inhibition of hypochlorite reduction by $Cr(OH)_3$ and Cr_2O_3 was independent of the film thickness, morphology and molecular structure indicated that the blocking mechanism is related to the chemical and electrochemical features of Cr(III) oxide-like films. The blocking mechanism was first rationalized to be due to a combined effect of surface charge and the semiconducting properties of Cr(III) oxides, although these effects do not apply to the thin in situ-formed films.

This mechanism was studied from a thermodynamic point of view using DFT calculations. It was shown that the adsorption of hypochlorite was thermodynamically feasible on both Cr and Fe. When the mechanism was further examined, clear differences appeared between Fe and Cr in a later step, namely, the recovery of the active site from a TM – OH state. DFT calculations showed that the reduction of Cr – OH, leading to the recovery of the "free" Cr active site, requires a large amount of energy and is not achievable under the potential at which water reduction occurs. The active site for hypochlorite reduction is, therefore, blocked by OH. On the other hand, Cr – OH sites are active to drive the HER, resulting in the selectivity observed experimentally.

In summary, this study has given a new insight into the selective mechanism provided by Cr(III) oxide-like films. The proposed mechanism can be used to design new selective electrodes,

enabling the removal of Cr(VI) from the chlorate process. These findings may also be applicable to studies on selectivity in other water reduction and H_2-producing processes.

8. Recommendations for replacing Cr(VI)

The vital selectivity provided by $Cr(OH)_3$ and Cr_2O_3 films was clearly shown to originate in the mechanisms of the hypochlorite and water reduction reactions. This information is extremely relevant to those who strive to remove sodium dichromate from the chlorate process. A suitable replacement for Cr(VI) should provide selectivity based on the same properties displayed by the Cr(III) on the electrode surface.

Performing the chlorate process without Cr(VI) (based on the technology existing today) is desired. Possible candidates to replace Cr, as a necessary component in the electrolyte, are likely located closely to Cr in the periodic table. Some of these candidates, such as molybdenum, have been studied for this specific function [49, 50, 118]. Others, such as manganese and vanadium, are mentioned in patents [119, 120] and not thoroughly described in fundamental studies. These elements could express the low nobility needed to strongly bind oxygen and enable OH blocking. However, their effects on the HER are unpredictable, as their compatibility with process conditions.

The development of selective cathodes could be an alternative if no additives work. However, this approach involves extensive work in material science to mimic the striking characteristics of Cr(III) with a new material. Moreover, the new material should be stable during electrolysis and not oxidized by hypochlorite and chlorate during shutdowns, as is the case for Cr(III) films (which are recovered under polarization).

Another alternative is the use of Cr(VI) at low concentrations (on the order of mg dm^{-3}). This approach would require the use of a material more stable and corrosive-resistant than mild steel. Titanium, for example, is used in some technologies for chlorate production, and the amount of Cr needed to ensure high CCE is relatively low. However, the overpotential towards the HER is high, which significantly increase the specific power consumption. In addition, the Ti lifetime is short due to formation of Ti hydrides. Therefore, a material that ensures a constant surface area, yet exhibiting good activity towards the HER, could enable to decrease the concentration of sodium dichromate to the lowest possible level. The catalytic activity towards the HER would be beneficial, but it is not necessary, since the formation of the Cr film could itself lower the overpotential, as it does on Au electrodes.

All the above mentioned suggestions disregard the other benefits provided by Cr(VI) for chlorate formation, such as: corrosion protection, buffering and being a homogeneous catalyst. Therefore, a complete study of the impact of removing Cr(VI) from the electrolyte must be included, when considering any possible replacements. This thesis provides new knowledge of the selectivity, but a solution for the Cr(VI) issue remains as a challenge for today's chlorate production technologies.

Acknowledgements

This thesis had the contribution of so many people that is difficult to choose the right order to thank. The order of appearance has nothing to do with the order of importance. Also, I know that I will end up forgetting to mention many of you, so please don't take it personal, I just finished my Thesis.

I think there is no more appropriate and batter way to start than thanking my supervisor, Elisabet Ahlberg. Definitely, this work would never reach so far without your insistence, dedication, discussions, demands and, on top of all, your knowledge, your patience, support and your invaluable scientific contributions. Stressful moments (who doesn't have it?) were all well compensated by all the learnings, the discoveries, the publications and, of course, this Thesis. What a journey! Thank you for your company during hard working days and in the good times we spent together.

Of course, nothing would be possible without great people from AkzoNobel. There is no way I can measure how much Mats Wildlock and Nina Simic have contributed to this work. Both of you have struggled and spent so much time working on my papers and on this Thesis, that I can say you are co-authors. Your scientific inputs and your support throughout the whole time, especially last year, were paramount for the completion of this work. It is hard to find words to express how much I am thankful!

I also want to thank Rolf Edvinsson and Pablo Wiedenbrug for hiring me. I thank Johan Wanngård who received and patiently introducing me to the chlorate world, and contributed a lot to this project. I take the opportunity to also thank all the colleagues from the pRD&I who received me with open arms and had (and still have ☺) patience to switch between Swedish and English in my presence. Passing members, as Katarzyna and Jun, my first friends in Gothenburg, are also very worthy to be mentioned. You all played a very important role, even if you haven't noticed it! Tack så jättemycket!!

Vasco and Cesar, you guys already have a special place in my s2. Thank you for the recent but strong friendship we built. Thank you also for speaking Portuguese. VALEU! haha!

I would like to thanks Mats (again!) and also Kalle Pelin for being outstanding bosses. Thanks for working so hard behind the curtains and for hiring me permanently. I know you played a priceless role. If there were more bosses like you, the world would be a better place!

At the University of Gothenburg I want, first of all, to thank Zareen Abbas for the friendship throughout these years. It is also thanks to your support that I got this far. I will definitely miss the fun talks during *fika*, covering mostly science, sports, world politics and memorable anecdotes. I have been enlightened by your knowledge, and I hope we can keep close contact. I am especially grateful also because you were the first to open the doors for Milene to integrate in the Swedish academic world, and I have no words to express it. Thank you very much!

I always complained about not having a lab technician in our group, but I think I bothered Gert Göransson enough times to fulfil the gap ☺. If it wasn't for you, my Ph.D. life would have been much harder. Thank you for all the assistance. Of course, the friendship we built during this time will be unforgettable. You were also a good company for a coffee, lunch breaks and beers (let's meet more often!).

I would like also to thank Christian Sögaard. You have been a great friend and colleague, and had the great idea of our Monthly Electrochemistry Afterwork (haha!). Thank you a lot for listening so patiently to so many complains last year. You definitely shared a little bit of my burden and helped me to keep going!

In general, I would like to thank all of those who have been part of the Electrochemistry group during these years. Special thanks go to Isabell and Krzysztof, who just arrived to the group, but I'll definitely miss! Michael Busch, for all the contributions with DFT calculations and for being a co-author in three out of five papers in this thesis. What a

privilege working with you. Thank you Patrik Steegstra for the nice chats in the short time we shared offices, and thank you for helping me with SEM/EDX and Nova. The invited students Mark (Mr. Sunshine) and Thomas (the silent), you were great companies. Thank you! Finally, my good friend and co-author Patrik Larses, thank you a lot for challenging me with tough questions and for the good times we spent together!

Two guys who deserve special attention in this chapter are Kristoffer Hedenstedt and Andrea Boschin. It was definitely an interesting journey to have you guys by my side. Kristoffer, you have been a great friend, and contributed a lot to build my knowledge on the scientific and engineering aspects of the chlorate production. Andrea, even if science were seldom the focus of our discussions, I learned valuable things you. Believe me, I did! On top of that, we really shared many legendary moments. I hope there are more to come. Thank you guys for your friendship!

I have to say that I always been the one to have many friends, but I think Milene has overcome me when she joined the Applied Chemistry group. Luckily, I was well received by all of them and this paragraph I dedicate to you Chalmers people from the 2nd and 3rd floor. I could say some names here, but I might be unfair. So I'll keep it general. Anyway, thanks a lot guys! You are the best group someone's wife could have.

From the University of Milano, I have a special thanks to Alberto Visibile for the friendship during your time in Gothenburg.

I would love to thank all my friends from Pederneiras, Piracicaba, São Carlos e Gothenburg. You all play a big role in my life! Missing you a lot!

Thanks to the great people from Haga Taekwondo! KI-RAB!!

I dedicate the last part to thank my family. I start thanking my father (*in memorian*) who taught me a lot about life, and never had the chance to know his son would become a Ph.D.. I thank my mother, who is the biggest example in my life. Your story is inspiring and you are the one to blame on my success. Thank you so much! My sisters, Gisela and Aline; my brothers(-in-law), Alexandre and Paulinho; and my nephews, Jessica, Leonardo and Rafael. Thank you for all the love and the prayers. I love you so much! Thank you all uncles and cousins, you also have part on it! Thanks for being part of my life.

The family Zezzi and family do Valle, I am so grateful and thankful because you have received as a son, a brother, a nephew, a grandson, an uncle. I want to thank each of you: vó Terezinha, tio Ulisses, tia Cássia, André, Dal, Marcelo, Alice e Amanda. I love you all. Special thanks tom my parents-in-law, Carlos and Marisa, who trust me to take care of their dotter, and allowed her, first, to merry and, and second, to bring her with me in this crazy journey. I love you!

Last but definitely not least, I thank my wife, Milene. You are my life, my joy, my strength, my motivation, my example, my inspiration and my happiness. I could not have done it without you. You supported me when all my pillars have fallen into pieces, and helped me to get over all the challenges of my adult life. I would love to have the words, but not even in Portuguese I could express all my gratitude. Thank you so much! Thank you for everything. Thank you for our baby. And thank you, Daniel, because I already love you. I love you two from the bottom of my heart.

Above all, I thank God for life and inspiration.

References

[1] H. Vogt, J. Balej, J. E. Bennett, P. Wintzer, S. A. Sheikh, P. Gallone, *et al.*, "Chlorine Oxides and Chlorine Oxygen Acids," in *Ullman's encyclopedia for industrial chemistry*, ed. Weinheim: Wiley-VHC Verlag, 2010.

[2] M. J. M. C. Barroca, P. J. T. S. Marques, I. M. Seco, and J. A. A. M. Castro, "Selectivity studies of oxygen and chlorine dioxide in the pre-delignification stages of a hardwood pulp bleaching plant," *Industrial and Engineering Chemistry Research*, vol. 40, pp. 5680-5685, 2001.

[3] P. Axegård and E. Bergnor. (2011). *Environmental performance of modern ECF bleaching.*

[4] S. Vogt, "Electrosynthesis of chlorate in the nineteenth century " *Journal of the Electrochemical Society*, vol. 128, pp. 29-32, 1981.

[5] S. Trasatti, "Electrocatalysis: understanding the success of DSA®," *Electrochimica Acta*, vol. 45, pp. 2377-2385, 2000.

[6] S. Trasatti, "Electrocatalysis in the anodic evolution of oxygen and chlorine," *Electrochimica Acta*, vol. 29, pp. 1503-1512, 1984.

[7] S. Trasatti, "Progress in the understanding of the mechanism of chlorine evolution at oxide electrodes," *Electrochimica Acta*, vol. 32, pp. 369-382, 3// 1987.

[8] H. B. Beer, "The invention and industrial-development of metal anodes," *Journal of the Electrochemical Society*, vol. 127, pp. C303-C307, 1980.

[9] A. Cornell, G. Lindbergh, and D. Simonsson, "The effect of adittion of chromate on the hydrogen evolution reaction and on iron oxidation in hydroxide and chlorate solutions," *Electrochimica Acta*, vol. 37, pp. 1873-1881, Aug 1992.

[10] B. V. Tilak, K. Tari, and C. L. Hoover, "Metal anodes and hydrogen cathodes: their activity towards O_2 evolution and ClO_3^- reduction reactions," *Journal of the Electrochemical Society*, vol. 135, pp. 1386-1392, 1988.

[11] G. Lindbergh and D. Simonsson, "The effect of chromate addition on cathodic reduction of hypochlorite in hydroxide and chlorate solutions," *Journal of the Electrochemical Society*, vol. 137, pp. 3094-3099, 1990.

[12] G. Lindbergh and D. Simonsson, "Inhibition of the cathode reactions in sodium hydroxide solution containing chromate," *Electrochimica Acta*, vol. 36, pp. 1985-1994, 1991.

[13] A. A. Tidblad and G. Lindbergh, "Surfaces analysis with ESCA and GD-OES of the film formed by cathodic reduction of chromate," *Electrochimica Acta*, vol. 36, pp. 1605-1610, 1991.

[14] L. Nylén and A. Cornell, "Effects of electrolyte parameters on the iron/steel cathode potential in the chlorate process," *Journal of Applied Electrochemistry*, vol. 39, pp. 71-81, 2009.

[15] J. Wullf and A. Cornell, "Cathodic current effiency in the chlorate process," *Journal of Applied Electrochemistry*, vol. 37, pp. 181-186, 2007.

[16] C. Wagner, "The cathodic reduction of anions and the anodic oxidation of cattions," *Journal of the Electrochemical Society*, vol. 101, pp. 181-184, 1954.

[17] R. Edvinsson-Albers and K. Hedenstedt, United States Patent US 20130292261 A1, 2013.

[18] F. Foerster and E. Muller, "Article on the theory of the electrolysis of alkali chloride solutions," *Zeitschrift fur elektrochemie*, vol. 9, pp. 171-185, 1903.

[19] I. M. Kolthoff and A. M. Shams El Din, "Reduction of hexavalent chromium at the rotated platinum electrode. Permeability of the film formed," *Journal of Physical Chemistry*, vol. 60, pp. 1564-1568, 1956.

[20] A. Leonárd and R. R. Lauwerys, "Carcinogenicity and mutagenicity of chromium," *Mutation Research*, vol. 76, pp. 227-239, 1980.

[21] A. Cornell and D. Simonsson, "Ruthenium dioxide as cathode material for hydrogen evolution in hydroxide and chlorate solutions," *Journal of the Electrochemical Society*, vol. 140, pp. 3123-3129, 1993.

[22] J. Gustavsson, L. Nylén, and A. Cornell, "Rare earth metal salts as potential alternatives to Cr(VI) in the chlorate process," *Journal of Applied Electrochemistry*, vol. 40, pp. 1529-1536, 2010/08/01 2010.

[23] L. Nylén, J. Gustavsson, and A. Cornell, "Cathodic Reactions on an Iron RDE in the Presence of Y(III)," *Journal of the Electrochemical Society*, vol. 155, pp. E136-E142, 2008.

[24] M. Li, Z. Twardowski, F. Mok, and N. Tam, "Sodium molybdate—a possible alternate additive for sodium dichromate in the electrolytic production of sodium chlorate," *Journal of Applied Electrochemistry*, vol. 37, pp. 499-504, 2007.
[25] U. C. Lačnjevac, B. M. Jović, L. M. Gajić-Krstajić, J. Kovač, V. D. Jović, and N. V. Krstajić, "Ti substrate coated with composite Cr-MoO_2 coatings as highly selective cathode materials in hypochlorite production," *Electrochimica Acta*, vol. 96, pp. 34-42, 2013.
[26] REACH, "Commision regulation (EU)," vol. No 348/2013 (2013).
[27] A. Cornell, "Chlorate Synthesis Cells and Technology, in Encyclopedia of Applied Electrochemistry." vol. 1, G. Kreysa, K.-i. Ota, and R. F. Savinell, Eds., ed: Springer-Verlag New York, 2014.
[28] J. W. Schumacher, R. Bradley, A. Leder, and N. Takei, *The Chemical Economics Handbook-SRI International*, 1999.
[29] K. Hedenstedt, "Electrochemical investigations of water and hypochlorite reduction on α-and γ-FeOOH," Licentiate, Department of Chemistry and Molecular Biology, University of Gothenburg, Gothenburg, 2015.
[30] K. Viswanathan and B. V. Tilak, "Chemical, electrochemical, and technological aspects of sodium chlorate manufacture," *Journal of the Electrochemical Society*, vol. 131, pp. 1551-1559, 1984.
[31] A. Cornell, B. Hakansson, and G. Lindbergh, "Ruthenium based DSA((R)) in chlorate electrolysis - critical anode potential and reaction kinetics," *Electrochimica Acta,* vol. 48, pp. 473-481, Jan 2003.
[32] A. Cornell, B. Hakansson, and G. Lindbergh, "Ruthenium-based dimensionally stable anode in chlorate electrolysis - Effects of electrolyte composition on the anode potential," *Journal of the Electrochemical Society*, vol. 150, pp. D6-D12, Jan 2003.
[33] K. Hedenstedt, "Energy efficiency in the sodium chlorate process," Doctor of Philosophy Doctoral Thesis, Department of Chemistry and Molecular Biology, University of Gothenburg, Gothenburg, 2017.
[34] J. E. Colman, "Electrolytic production of sodium chlorate," *American Institute of Chemical Engineers Symposium Series*, vol. 77, pp. 244-263, 1981.
[35] D. C. Harris, *Exploring Chemical Analysis*, 4th ed. New York: W. H. Freeman, 2009.
[36] N. N. Greenwood and A. Earnshaw, *Chemistry of the elements*, Second Edition ed. vol. 1: Elsevier, 1997.
[37] K. L. Hardee and L. K. Mitchell, "The influence of electrolyte parameters on the percent of oxygen evolved from a chlorate cell," *Journal of the Electrochemical Society*, vol. 136, pp. 3314-3318, Nov 1989.
[38] B. V. Tilak, K. Viswanathan, and C. G. Rader, "On the mechanism of sodium-chlorate formation," *Journal of the Electrochemical Society*, vol. 128, pp. 1228-1232, 1981.
[39] M. Spasojevic, N. Krstajic, and M. Jaksic, "Electrocatalytic optimization of faradaic yields in the chlorate cell process," *Surface Technology*, vol. 21, pp. 19-26, 1984.
[40] B. Endrodi, N. Simic, M. Wildlock, and A. Cornell, "A review of chromium(VI) use in chlorate electrolysis: Functions, challenges and suggested alternatives," *Electrochimica Acta*, vol. 234, pp. 108-122, Apr 2017.
[41] W. J. Clark and R. L. McCreery, "Inhibition of corrosion-related reduction processes via chromium monolayer formation," *Journal of the Electrochemical Society*, vol. 149, pp. B379-B386, Sep 2002.
[42] K. Hedenstedt, N. Simic, M. Wildlock, and E. Ahlberg, "Current efficiency of individual electrodes in the sodium chlorate process: a pilot plant study," *Journal of Applied Electrochemistry*, vol. 47, pp. 991-1008, 2017.
[43] M. Spasojević, D. Marković, T. Trišović, and M. Spasojević, "Mathematical model of the catalytic effect of chromium(VI) on hypochlorite disproportionation in chlorate electrolysis," *Journal of the Electrochemical Society*, vol. 165, pp. E8-E19, 2018.
[44] J. Wanngård and M. Wildlock, "The catalyzing effect of chromate in the chlorate formation reaction," *Chemical Engineering Research and Design*, vol. 121, pp. 438-447, 5// 2017.
[45] A. Ahlberg Tidblad and J. Mårtensson, "*In situ* ellipsometric characterization of the films formed by cathodic reduction of chromate," *Electrochimica Acta*, vol. 42, pp. 389-398, 1997.
[46] I. Taniguchi and T. Sekine, *Denki Kagaku*, vol. 43, pp. 201-208, 1975.

[47] B. E. Wilde and F. G. Hodge, "The cathodic discharge of hydrogen on active and passive chromium surfaces in dilute sulfuric acid solutions," *Electrochimica Acta*, vol. 14, pp. 619-627, 1969.
[48] E. Muller, "Uber ein elektrolytisches verfawren zur gewinnung der chlor-, brom- und jodsauren salze der alkalien," *Zeitschrif für elektrochemie*, vol. 5, pp. 469-473, 1899.
[49] J. Gustavsson, G. Lindbergh, and A. Cornell, "In-situ activation of hydrogen evolution in pH-neutral electrolytes by additions of multivalent cations," *International Journal of Hydrogen Energy*, vol. 37, pp. 9496-9503, Jun 2012.
[50] J. Gustavsson, G. Li, C. Hummelgård, J. Bäckström, and A. Cornell, "On the suppression of cathodic hypochlorite reduction by electrolyte additions of molybdate and chromate ions," *Journal of Electrochemical Science and Engineering*, vol. 2, pp. 185-198, 2012.
[51] M. Yoshida, K. Takanabe, K. Maeda, A. Ishikawa, J. Kubota, Y. Sakata, *et al.*, "Role and Function of Noble-Metal/Cr-Layer Core/Shell Structure Cocatalysts for Photocatalytic Overall Water Splitting Studied by Model Electrodes," *Journal of Physical Chemistry C*, vol. 113, pp. 10151-10157, Jun 2009.
[52] C. M. A. Brett and A. M. O. Brett, "Mass Transport," in *Electrochemistry: principles, methods and applications*, ed New York: Oxford University Press Inc., 1993, pp. 82-102.
[53] A. J. Bard and L. R. Faulkner, "Potential Sweep Methods," in *Electrochemical Methods: Fundamentals and Applications*, 2 ed United States of America: John Wiley & Sons, 2001, pp. 226-260.
[54] A. J. Bard and L. R. Faulkner, "Introduction and Overview of Electrode Processes," in *Electrochemical Methods: Fundamentals and Applications*, 2 ed United States of America: John Wiley & Sons, 2001, pp. 1-43.
[55] E. Ahlberg and H. Anderson, "AC impedance of the amalgamated zinc electrode," *Acta Chemica Scandinavian*, vol. 47, pp. 1063-1070, 1993.
[56] NanoScience. *Scanning Electron Microscopy*. Available: http://www.nanoscience.com/technology/sem-technology/
[57] R. Jenkins and R. L. Snyder. (1996). *Introduction to X-ray powder diffractometry*. *138*.
[58] A. J. Bard and L. R. Faulkner, "Spectrochemistry and Other Coupled Characterization Methods," in *Electrochemical Methods: Fundamentals and Applications*, 2 ed United States of America: John Wiley & Sons, 2001, pp. 680-735.
[59] J. R. Ferraro, K. Nakamoto, and C. W. Brown, "Basic Theory," in *Introductory Raman Sctroscopy*, Second ed Amsterdan;Boston: Academic Press, 2003, pp. 1-94.
[60] P. J. Haines, "Thermogravimetry," in *Thermal Methods of Analysis: Principles, Applications and Problems* ed London: Springer, Dordrecht, 1995, pp. 22-62.
[61] P. J. Haines and F. W. Wilburn, "Differential Thermal Analysis and Differential Scanning Calorimetry," in *Thermal Methods of Analysis: Principles, Applications and Problems* ed London: Springer, Dordrecht, 1995, pp. 63-122.
[62] M. Aguilar, E. Barrera, M. Palomar-Pardavé, L. Huerta, and S. Muhl, "Characterization of black and white chromium electrodeposition films: surface and optical properties," *Journal of Non-Crystalline Solids*, vol. 329, pp. 31-38, 11/1/ 2003.
[63] H. A. Duarte, K. Jha, and J. W. Weidner, "Electrochemical reduction of nitrates and nitrites in alkaline media in the presence of hexavalent chromium," *Journal of Applied Electrochemistry*, vol. 28, pp. 811-817, Aug 1998.
[64] J. J. Hatch and A. A. Gewirth, "Potential Dependent Chromate Adsorption on Gold," *Journal of the Electrochemical Society*, vol. 156, pp. D497-D502, 2009.
[65] A. K. Bairamow, S. Zakipour, and C. Leygraf, "An XPS investigation of dichromate and molybdate inhibitors on aluminum," *Corrosion Science*, vol. 25, pp. 69-73, 1985.
[66] M. Aguilar-Sánchez, M. Palomar-Pardavé, M. Romero-Romo, M. T. Ramírez-Silva, E. Barrera, and B. R. Scharifker, "Electrochemical nucleation and growth of black and white chromium deposits onto stainless steel surfaces," *Journal of Electroanalytical Chemistry*, vol. 647, pp. 128-132, 9/1/ 2010.
[67] D. Rai, D. A. Moore, N. J. Hess, K. M. Rosso, L. Rao, and S. M. Heald, "Chromium(III) hydroxide solubility in the aqueous K+-H+-OH--CO2-HCO3--CO32--H2O system: A thermodynamic model," *Journal of Solution Chemistry*, vol. 36, pp. 1261-1285, Oct 2007.

[68] D. Rai, B. M. Sass, and D. A. Moore, "Chromium(III) hydrolysis constants and solubility of chromium(III) hydroxide," *Inorganic Chemistry*, vol. 26, pp. 345-349, Feb 1987.
[69] S. M. El-Sheikh, R. M. Mohamed, and O. A. Fouad, "Synthesis and structure screening of nanostructured chromium oxide powders," *Journal of Alloys and Compounds*, vol. 482, pp. 302-307, 2009.
[70] H. J. Gulley-Stahl, W. L. Schmidt, and H. A. Bullen, "Characterization and reactivity of chromia nanoparticles prepared by urea forced hydrolysis," *Journal of Materials Science*, vol. 43, pp. 7066-7072, 2008.
[71] P. Li, Z. Zhou, H. Xu, and Y. Zhang, "A novel hydrolysis method to synthesize chromium hydroxide nanoparticles and its catalytic effect in the thermal decomposition of ammonium perchlorate," *Thermochimica Acta*, vol. 544, pp. 71-76, 2012.
[72] Z. Pei and Y. Zhang, "A novel method to prepare Cr2O3 nanoparticles," *Materials Letters*, vol. 62, pp. 504-506, 2008.
[73] H. Xu, T. Lou, and Y. Li, "Synthesis and characterize of trivalent chromium $Cr(OH)_3$ and Cr_2O_3 microspheres," *Inorganic Chemistry Communications*, vol. 7, pp. 666-668, 2004.
[74] S. Lei, X. Peng, Z. Liang, X. Li, C. Wang, B. Cheng, *et al.*, "Self-template formation and properties study of Cr 2O 3 nanoparticle tubes," *Journal of Materials Chemistry*, vol. 22, pp. 1643-1651, 2012.
[75] Z. Xie, J. Fan, Y. Cheng, L. Jin, G. Hu, J. Lu, *et al.*, "Cr_2O_3 catalysts for fluorination of 2-Chloro-3,3,3-trifluoropropene to 2,3,3,3-tetrafluoropropene," *Industrial and Engineering Chemistry Research*, vol. 52, pp. 3295-3299, 2013.
[76] S. Eugenio, C. M. Rangel, R. Vilar, and A. M. B. do Rego, "Electrodeposition of black chromium spectrally selective coatings from a Cr(III)-ionic liquid solution," *Thin Solid Films*, vol. 519, pp. 1845-1850, Jan 2011.
[77] Z. A. Hamid, "Electrodeposition of black chromium from environmentally electrolyte based on trivalent chromium salt," *Surface & Coatings Technology*, vol. 203, pp. 3442-3449, Aug 2009.
[78] S. Jafari and M. Rozati, "Characterization of black chrome films prepared by electroplating technique," *World Renewable Energy Congress - 2011*, 2011.
[79] N. Vasudevan, V. K. W. Grips, and I. Rajagopalan, "The present status of black chromium plating," *Surface Technology*, vol. 14, pp. 119-132, 1979.
[80] F. D. Hardcastle and I. E. Wachs, "Raman spectroscopy of chromium oxide supported on Al_2O_3, TiO_2 and SiO_2: a comparative study," *Journal of Molecular Catalysis*, vol. 46, pp. 173-186, 1988.
[81] J. Birnie, C. Craggs, D. J. Gardiner, and P. R. Graves, "Ex situ and in situ determination of stress distributions in chromium oxide films by raman microscopy," *Corrosion Science*, vol. 33, pp. 1-12, 1992.
[82] J. Mougin, T. Le Bihan, and G. Lucazeau, "High-pressure study of Cr2O3 obtained by high-temperature oxidation by X-ray diffraction and Raman spectroscopy," *Journal of Physics and Chemistry of Solids*, vol. 62, pp. 553-563, 2001.
[83] J. Yang, W. N. Martens, and R. L. Frost, "Transition of chromium oxyhydroxide nanomaterials to chromium oxide: A hot-stage Raman spectroscopic study," *Journal of Raman Spectroscopy*, vol. 42, pp. 1142-1146, 2011.
[84] T. Ivanova, K. A. Gesheva, M. Kozlov, and M. Abrashev, "Electrochromic and optical study of atmospheric pressure chemical vapour deposition MoO 3-Cr 2O 3 films," *Journal of Nanoscience and Nanotechnology*, vol. 11, pp. 8017-8023, 2011.
[85] C. A. Melendres, M. Pankuch, Y. S. Li, and R. L. Knight, "Surface enhanced Raman spectroelectrochemical studies of the corrosion films on iron and chromium in aqueous solution environments," *Electrochimica Acta*, vol. 37, pp. 2747-2754, 1992.
[86] I. M. B. Nielsen and M. D. Allendorf, "Thermochemistry of the chromium hydroxides Cr(OH)(n), n=2-6, and the oxyhydroxide CrO(OH)4: Ab initio predictions," *Journal of Physical Chemistry A*, vol. 110, pp. 4093-4099, Mar 2006.
[87] A. V. Baranov, K. V. Bogdanov, A. V. Fedorov, M. V. Yarchuk, A. I. Ivanov, V. P. Veiko, *et al.*, "Micro-Raman characterization of laser-induced local thermo-oxidation of thin chromium films," *Journal of Raman Spectroscopy*, vol. 42, pp. 1780-1783, 2011.
[88] Q. Dong, J. Hu, Z. Guo, J. Lian, J. Chen, and B. Chen, "Surface morphology study on chromium oxide growth on Cr films by Nd-YAG laser oxidation process," *Applied Surface Science*, vol. 202, pp. 114-119, 2002.

[89] Q. Dong, J. Hu, J. Lian, Z. Guo, J. Chen, and B. Chen, "Oxidation behavior of Cr films by Nd:YAG pulsed laser," *Scripta Materialia*, vol. 48, pp. 1373-1377, 2003.
[90] J. Lian, Q. Dong, Z. Guo, Q. Xu, J. Yang, J. Hu, *et al.*, "Surface oxidation kinetics of Cr film by Nd-YAG laser," *Materials Science and Engineering A*, vol. 391, pp. 210-220, 2005.
[91] C. Y. Cui, C. D. Xia, X. G. Cui, J. Z. Zhou, X. D. Ren, and Y. M. Wang, "Novel morphologies and growth mechanism of Cr2O3 oxide formed on stainless steel surface via Nd: YAG pulsed laser oxidation," *Journal of Alloys and Compounds*, vol. 635, pp. 101-106, 2015.
[92] L. Kotsedi, Z. Y. Nuru, P. Mthunzi, T. F. G. Muller, S. M. Eaton, B. Julies, *et al.*, "Femtosecond laser surface structuring and oxidation of chromium thin coatings: Black chromium," *Applied Surface Science*, vol. 321, pp. 560-565, 2014.
[93] S. Beauvais-Réveillon, A. M. Huntz, G. Moulin, and J. J. Bléchet, "Comparison of classical oxidation and laser oxidation of a chromium PVD coating on a pure-iron substrate," *Oxidation of Metals*, vol. 43, pp. 279-300, 1995.
[94] B. Fazio, L. Spadaro, G. Trunfio, J. Negro, and F. Arena, "Raman scattering of MnOx-CeOx composite catalysts: Structural aspects and laser-heating effects," *Journal of Raman Spectroscopy*, vol. 42, pp. 1583-1588, 2011.
[95] J. D. Carruthers, K. S. W. Sing, and J. Fenerty, "Glow phenomenon of chromium oxide," *Nature*, vol. 213, pp. 66-68, 1967.
[96] Z. Huang, C. Chen, J. Xie, and Z. Wang, "The evolution of dehydration and thermal decomposition of nanocrystalline and amorphous chromium hydroxide," *Journal of Analytical and Applied Pyrolysis*, vol. 118, pp. 225-230, 3// 2016.
[97] S. Kittaka, T. Morooka, K. Kitayama, and T. Morimoto, "Thermal decomposition of chromium-oxide hydroxide I. Effect of particle-size and atmosphere," *Journal of Solid State Chemistry*, vol. 58, pp. 187-193, 1985.
[98] S. Kittaka and T. Tahara, "Thermal decomposition of chromium oxide hydroxide," *Journal of Colloid and Interface Science*, vol. 112, pp. 252-260, 1986/07/01 1986.
[99] S.-t. Liang, H.-l. Zhang, M.-t. Luo, K.-j. Luo, P. Li, H.-b. Xu, *et al.*, "Colour performance investigation of a Cr2O3 green pigment prepared via the thermal decomposition of CrOOH," *Ceramics International*, vol. 40, pp. 4367-4373, 4// 2014.
[100] S. Musić, M. Maljković, S. Popović, and R. Trojko, "Formation of chromia from amorphous chromium hydroxide," *Croatica Chemica Acta*, vol. 72, pp. 789-802, 1999.
[101] K. Hedenstedt, J. Bäckström, and E. Ahlberg, "In-Situ Raman spectroscopy of α- and γ-FeOOH during cathodic load," *Journal of Electrochemistry Society*, vol. 164, pp. H621-H627, 2017.
[102] Y. Z. Tang, F. M. Michel, L. H. Zhang, R. Harrington, J. B. Parise, and R. J. Reeder, "Structural Properties of the Cr(III)-Fe(III) (Oxy)hydroxide Compositional Series: Insights for a Nanomaterial "Solid Solution"," *Chemistry of Materials*, vol. 22, pp. 3589-3598, Jun 2010.
[103] S. M. Walker, M. C. Marcano, W. M. Bender, and U. Becker, "Imaging the reduction of chromium(VI) on magnetite surfaces using in situ electrochemical AFM," *Chemical Geology*, vol. 429, pp. 60-74, 2016.
[104] U. Schwertmann, U. Gasser, and H. Sticher, "Chromium-for-iron substitution in synthetic goethites," *Geochimica et Cosmochimica Acta*, vol. 53, pp. 1293-1297, 1989.
[105] A. Cornell, "Chlorate Cathodes and Electrodes Design, in Encyclopedia of Applied Electrochemistry." vol. 1, G. Kreysa, K.-i. Ota, and R. F. Savinell, Eds., ed: Springer-Verlag New York, 2014.
[106] T. Hiemstra, W. H. Van Riemsdijk, and G. H. Bolt, "Multisite proton adsorption modeling at the solid/solution interface of (hydr)oxides: A new approach. I. Model description and evaluation of intrinsic reaction constants," *Journal of Colloid And Interface Science*, vol. 133, pp. 91-104, 1989.
[107] M. Kosmulski, "pH-dependent surface charging and points of zero charge. III. Update," *Journal of Colloid and Interface Science*, vol. 298, pp. 730-741, 2006.
[108] M. Kosmulski, "Compilation of PZC and IEP of sparingly soluble metal oxides and hydroxides from literature," *Advances in Colloid and Interface Science*, vol. 152, pp. 14-25, 2009.
[109] M. Kosmulski, "Isoelectric points and points of zero charge of metal (hydr)oxides: 50years after Parks' review," *Advances in Colloid and Interface Science*, vol. 238, pp. 1-61, 2016/12/01/ 2016.
[110] A. E. Onjia, S. K. Milonjic, D. Cokesa, M. Comor, and N. Miljevic, "Characterization of colloidal chromia particles obtained by forced hydrolysis," *Materials Research Bulletin*, vol. 38, pp. 1329-1339, Jul 2003.

[111] H. Asteman, E. Ahlberg, and J.-E. Svensson, "Electric Properties of Alpha Fe2O3, Cr2O3, and a(Fe,Cr)2O3, and Their Relevance to Corrosion," *Electrochemical Society*, vol. 99 - 38, pp. 17-25, 1999.
[112] N. E. Hakiki, "Influence of surface roughness on the semiconducting properties of oxide films formed on 304 stainless steel," *Journal of Applied Electrochemistry*, vol. 38, pp. 679-687, 2008.
[113] P. C. Searson and R. M. Latanision, "A photoelectrochemical study of the passive film on chromium," *Electrochimica Acta*, vol. 35, pp. 445-450, 1990.
[114] H. Tsuchiya, S. Fujimoto, O. Chihara, and T. Shibata, "Semiconductive behavior of passive films formed on pure Cr and Fe-Cr alloys in sulfuric acid solution," *Electrochimica Acta*, vol. 47, pp. 4357-4366, 2002.
[115] J. C. F. Boodts and S. Trasatti, "Hydrogen evolution on iridium oxide cathodes," *Journal of Applied Electrochemistry*, vol. 19, pp. 255-262, 1989.
[116] N. Krstajic and S. Trasatti, "Cathodic behaviour of RuO2-doped Ni/Co3O4 electrodes in alkaline solutions: Hydrogen evolution," *Journal of Applied Electrochemistry*, vol. 28, pp. 1291-1297, 1998.
[117] E. Veggetti, I. M. Kodintsev, and S. Trasatti, "Hydrogen evolution on oxide electrodes: Co 3 O 4 in alkaline solution," *Journal Electroanalytical Chemistry*, vol. 339, pp. 255-268, 1992.
[118] J. Gustavsson, C. Hummelgård, J. Bäckström, I. O. Wallinder, S. M. H. Rahman, G. Lindbergh, *et al.*, "In-situ activated hydrogen evolution by molybdate addition to neutral and alkaline electrolytes," *Journal of Electrochemical Science and Engineering*, vol. 2, p. 105, 2012.
[119] O. Arimoto and T. Kishi, "Electrolytic method for manufacturing hypochlorite," United States Patent, 1995.
[120] E. R. Loftfield, "Bipolar diaphragmless electrolytic cells," United States Patent, 1975.